

POLITECNICO DI TORINO

Department of Mechanical, Aerospace, Automotive
and Production Engineering

Master of Science in Automotive Engineering

Master Degree Thesis

**Improvements of 3D-CFD
simulations of high-performance
multi-hole injectors**



Professor:

Prof. Federico Millo

Supervisors:

Dr. Ing. Marco Chiodi

M.Sc. Antonino Vacca

Candidate

Edoardo Rossi

Student ID: 243571

ACADEMIC YEAR 2018-2019

Abstract

The increasingly stringent regulations in terms of pollutant emissions have lead the automotive industry to concentrate its resources in the research not only of new propulsion technologies (e.g. electric vehicles), but also of new methods to improve internal combustion engine's efficiency while at least keeping the same performance. Particular attention has been given to the development of more precise and efficient fuel injection systems combined with suitable injection strategies, since a well targeted injection of the fuel in sufficient quantity and at the right time has a decisive influence on the subsequent processes of ignition, combustion and pollutant formation. One of the most powerful tools in the investigation of injection and mixture formation process is the 3D-CFD simulation, which can provide a very precise and reliable reproduction of thermo-fluid-dymanical phenomena inside the engine, with consequent savings in time and financial resources related to the not anymore necessary test campaigns.

The subject of this work is the study and the research of possible improvements of the injection model for 3D-CFD simulation, in the particular application of high-performance multi-hole injectors for Gasoline Direct Injection (GDI) applications. A set of experimental tests will provide the necessary support for the validation of a new, more precise injection model developed for the 3D-CFD tool *QuickSim*. The 3D-CFD tool *QuickSim* was developed at the Forschungsinstitut für Kraftfahrwesen und Fahrzeugmotoren Stuttgart (FKFS) and the Institut für Verbrennungsmotoren und Kraftfahrwesen (IVK) of the University of Stuttgart, on the base of the 3D-CFD commercial software Star-CD. Its peculiarity is the adoption of specifically designed models for combustion, heat transfer, etc. which lead to a consistent reduction in computational time, hence the possibility of performing full engine simulations over successive cycles in a time sufficiently short to allow the utilization of 3D-CFD simulation directly in the engine development process.

The starting point of this investigation is the analysis, by means of a developed imaging tool, of a set of experimental tests of fuel injection with a multi-hole injector at high injection pressure, which provides data about the spray formation and propagation inside a constant volume test chamber under different conditions of injection pressure and chamber pressure. The obtained data are then exploited in

the process of calibration of the injection initialization parameters of the 3D-CFD simulation. In fact *QuickSim*'s injection model does not include the simulation of internal nozzle flow and droplets primary breakup, and an initialization domain is present in which the properties of the injected droplets (velocity, diameter, target direction) are defined. The dependence of the simulation quality on the initialization parameters will be discussed, in order to provide a methodology for the selection of the best set of parameters. Furthermore a sensitivity analysis of the injection simulation to the injection conditions is performed, with particular focus on how the different models implemented for the description of secondary breakup and vaporization of the injected fuel influence the final results.

The validation of the developed methodology is performed again exploiting the experimental data obtained in the first phase of the work, and by means of the application of the new injection model to a case of full engine simulation.

In summary, this work is dedicated to the implementation of a set of guidelines for the definition of an injection model able to provide more precise and reliable injection simulations without affecting the computational effort required by the 3D-CFD software, taking into account its final application in the virtual engine development process.

Acknowledgements

This work is the results of my activity at Forschungsinstitut für Kraftfahrwesen und Fahrzeugmotoren Stuttgart (FKFS). I would like to express my deep gratitude to Prof. Federico Millo and Dr. Ing. Marco Chiodi for allowing me to produce my thesis work in FKFS, and for always giving me their expert advice when needed.

I would also like to offer my special thanks to all the 3D-CFD Simulation team in FKFS, and in particular to Antonino Vacca, who has supervised my work throughout its whole development, not only providing constant professional support, but also helping in having a pleasant time in the work environment.

I extend my thanks to all the people that I have known in Stuttgart, because they have allowed this experience not only to be rewarding from the academic point of view, but also to be an opportunity for personal growth.

Finally I would like to thank my family, who has always supported and encouraged me in these years of studies far from home, and has never hesitated in believing in my choices for the future.

Torino, 2019

Edoardo Rossi

Contents

Abstract	II
Acknowledgements	IV
1 Introduction	1
1.1 Gasoline Direct Injection	1
1.1.1 Multi-hole injectors for GDI	2
1.2 Engine future developments	4
1.2.1 Injection experimental analysis	5
1.2.2 3D-CFD simulation	6
1.3 Objective of the Thesis	8
1.3.1 Experimental tests analysis	9
1.3.2 3D-CFD simulation of injection	9
1.3.3 Improvements of 3D-CFD injection simulations	10
2 Experimental Tests Analysis	11
2.1 Experimental Set-up	11
2.2 Procedure and Investigated Quantities	13
2.2.1 Imaging Matlab Tool Description	14
2.3 Analysis Results	20
2.3.1 Spray Axial Penetration	20
2.3.2 Spray Vertical Penetration	22
2.3.3 Spray Angle	24
2.3.4 Spray Speed	26
2.3.5 Conclusions	27
3 3D-CFD Simulation of Injection - Software	31
3.1 3D-CFD software QuickSim	31
3.2 Fuel Injection Modeling in QuickSim	33
3.2.1 Spray atomization models	35
3.3 Performed Injection Simulations	38

4	3D-CFD Simulation of Injection - Calibration of Initialization Parameters	41
4.1	Fluid Exit Speed	42
4.2	Spray Angles and Initialization Domain	45
4.3	SMD of Initialization	46
4.4	Final Choices and Results	49
5	3D-CFD Simulation - Variation of Injection Conditions	53
5.1	Simulations Results with Variation of Injection Conditions	54
5.2	Fluids Behaviour Models	57
5.2.1	Breakup Models in <i>QuickSim</i>	57
5.2.2	Description of the Environment Fluid	61
5.3	Application of Different Breakup Models	62
5.3.1	Standard Injection Conditions	62
5.3.2	Variation in Injection Conditions	63
5.4	Modification of SMD of Initialization	68
5.5	ICE Simulations	71
6	Conclusions and Outlook	75
	Bibliography	79

List of Tables

2.1	Injectors characteristics	12
2.2	Tests summary	13
2.3	Summary of experimental tests analysis results	28
3.1	First choice of simulation's parameters	40
4.1	Speed calibration - numerical results	44
4.2	Calibration of initialization parameters - Final choice	50
5.1	SMD of initialization for best fitting - $P_r = 100$ [bar]	69

List of Figures

1.1	Gasoline Direct Injection system example [9]	3
1.2	Multi-hole solenoid injector for GDI by Bosch GmbH	4
2.1	Injector target points	12
2.2	Example of acquired frames of experimental video using Matlab tool showing the evolution in time of the spray.	15
2.3	Example of image processing of the injection video before the analysis	16
2.4	Analysed frame example	17
2.5	Analysis results plot	18
2.6	Spray propagation	19
2.7	Example of adaptation of the tool for the analysis of injection in different test chamber (water injection)	20
2.8	Spray Axial Penetration - Injector type F	21
2.9	Spray Axial Penetration - Injector type G	21
2.10	Comparison of spray axial penetration between injectors of type F and G in the case of $P_r = 200[bar]$ and $P_k = 5[bar]$	22
2.11	Spray vertical penetration for injector of type F as a function of Injection pressure and Chamber pressure	23
2.12	Comparison of spray vertical penetration between injectors of type F and G in the case of $P_r = 200[bar]$ and $P_k = 5[bar]$	24
2.13	Spray Angle for injector of type F as a function of Injection pressure and Chamber pressure	25
2.14	Comparison of spray angle between injectors of type F and G in the case of $P_r = 200[bar]$ and $P_k = 5[bar]$	26
2.15	Spray angle dispersion analysis - CV	26
2.16	Spray Speed	27
2.17	Example of spray propagation for the two types if injector - ZX plane	28
3.1	Spray angle definition	34
3.2	Definition of droplets initialization region	34
3.3	Spray atomization mechanisms [5]	36
3.4	Reitz-Diwakar breakup mechanisms	37
3.5	Combustion chamber model for 3D-CFD simulation	39

4.1	Initialization speed profile for standard injection conditions	43
4.2	Speed calibration results	43
4.3	Influence of initialization speed on SMD distribution	44
4.4	Initialization parameters variation	46
4.5	Results for simulation with higher SMD_{init}	47
4.6	Results for variable SMD of initialization	48
4.7	Calibration of initialization parameters - Final results	49
4.8	Analysed frames: Experiments (left) and Simulation (right)	51
5.1	Penetration curves - $P_r = 100$ [bar]	54
5.2	Penetration curves - $P_r = 200$ [bar]	54
5.3	Spray angle for $P_r = 100$ [bar], $P_k = 10$ [bar]	55
5.4	Speed vectors inside the chamber [m/s] - $P_r = 100$ [bar]	56
5.5	Turbulent Kinetic Energy inside the chamber [m^2/s^2] - $P_r = 100$ [bar]	56
5.6	Differences in the KH and RT breakup models	61
5.7	Penetration curves from simulations with different droplets breakup models	63
5.8	Results for simulation in standard injection conditions with KHRT breakup model	64
5.9	Droplets diameter distribution at 30 [mm] from injector tip - Standard injection conditions and different breakup models	64
5.10	Effects of breakup models in a variety of injection conditions	65
5.11	Effect of breakup model modification on the fuel vaporized mass	66
5.12	Effects of injection conditions on droplets diameter distribution	66
5.13	$P_r = 100$ [bar], $P_k = 5$ [bar] - Effects of breakup model deactivation	67
5.14	Penetration curves for simulations with adapted SMD of initialization	69
5.15	SMD of initialization as a function of chamber pressure	69
5.16	SMD of initialization and SMD distribution in a cross section of the spray at 30 [mm] from the injector tip	70
5.17	Example for $P_k = 5$ [bar] of Liquid and vaporized mass distribution - Comparison with the basic case	70
5.18	Spray propagation at End of Injection (EOI)	72
5.19	Liquid and Vaporized mass distributions	72
5.20	Lambda distribution at Ignition Point - Default settings	73
5.21	Lambda distribution at Ignition Point - New model	73

Chapter 1

Introduction

In the last few decades, the research on internal combustion engines and alternative propulsion systems has been crucial in the attempt to satisfy the increasingly demanding limitations in terms of fuel consumption and engine emissions. Different technologies have been studied and developed to improve the efficiency of internal combustion engines. One of the most important research topic in this field is the study of air/fuel mixture formation, and consequently the study of fuel injection system and injection strategy. This includes the investigation of alternative combustion modes, such as HCCI, and injection systems.

In the engine development process, these phenomena can be studied by means of experimental tests, mostly based on optical spray diagnostics, and accurate 3D-CFD simulations.

This work takes into account both experimental data and 3D-CFD simulations in the case of Gasoline Direct Injection (GDI) with high-performance multi-hole injectors, with the aim of improving the computational injection model exploiting experimental results.

The CFD simulations have been carried out using a 3D-CFD-simulation software developed by FKFS (Forschungsinstitut für Kraftfahrwesen und Fahrzeugmotoren Stuttgart) and IVK - University of Stuttgart (Institut für Verbrennungsmotoren und Kraftfahrwesen) called *Quicksim*, whose characteristics will be described in the following chapters.

1.1 Gasoline Direct Injection

Gasoline Direct Injection (GDI) is an advanced injection system for gasoline engines which allows to improve the control on mixture formation, thus combustion and engine's efficiency. The fuel spray is injected directly into the cylinder, generating an ignitable fuel/air mixture in proximity of the spark plug at ignition time. The

power output is controlled by varying the amount of fuel injected into the cylinder. This system can achieve higher efficiencies with respect to port fuel injection systems (PFI), but it has been possible to fully exploit its potential only after the spread of electronically controlled, high pressure injection systems (pressures higher than 100[bar]), which guarantee an high level of flexibility of the system.

Direct injection is characterized by the possibility of adjusting the injection strategy to the engine load conditions:

- Charge stratification can be obtained, especially at part load, by concentrating most of the fuel in the neighbourhood of the spark plug, so to achieve locally a close to stoichiometric mixture in an overall lean environment, which can be easily ignited. Under those circumstances engine throttling at part load can be avoided, thus significantly reducing pumping losses.
- Homogeneous mixture is desired at full load and in some part load operations. An homogeneous overall stoichiometric mixture can be obtained with early injection strategies, with benefits in terms of volumetric efficiency, transient response, peak torque and power, and combustion stability.

The progress in direct injection gasoline engines depends entirely on new injector technologies and the appropriate exploitation of the in-cylinder airflow. The latter is of great importance and is effectively reflected on the selected injection timing for achieving homogeneous, as well as, stratified engine operation. In other words, the development of a successful combustion system depends upon the optimised design of the fuel injection system, the proper matching of the system components and the careful development of injection timing maps, for the best possible exploitation of the in-cylinder airflow and the advantages it offers towards effective transportation of the desired fuel vapour clouds to the sprak-plug positions [2]. Figure 1.1 shows an example of modern gasoline direct injection system with injector in near position with respect to the spark plug.

1.1.1 Multi-hole injectors for GDI

Spark-ignition gasoline direct injection engines present several feasible design configurations, which are classified depending on the relative position of the injector to the spark-plug, which can be narrow-spacing or wide-spacing, the piston crown shape, the injection timing, and the air motion and mixture preparation strategy. In particular, the mixture cloud can be guided towards the spark-plug following three different methods, which are classified as: wall-guided, air-guided, or spray-guided combustion systems. Wall-guided combustion systems were the first used, where the injector was mounted in wide-spacing position, and the fuel spray was directed in such a way to match a specifically designed piston bowl's cavity responsible for the



Figure 1.1: Gasoline Direct Injection system example [9]

redirection of the ignitable cloud towards the spark-plug. Air-guided combustion systems were designed to overcome the undesirable effects of wall impingement of wall-guided systems. Anyway, these systems need a specific combustion chamber design in order to guarantee the correct airflow inside the cylinder. The most recent trend in DI is the adoption of spray-guided combustion systems, in which the mixture formation and motion is controlled by means of the high-pressure injector, which is in narrow-spacing position, and the need of complex combustion chamber's geometry is not an issue anymore.

It is possible to find in literature several studies mainly focused on swirl pressure atomizers, in which a swirling motion is imparted to the liquid so that it spreads out in the form of a conical sheet as soon as it leaves the orifice of the nozzle. This type of injector can produce very finely atomized droplets of fuel over a moderate range of injection pressures. The drawback of adopting this type of injector is that their spray is highly sensitive to the injection conditions (injection pressure and thermodynamic state inside the cylinder), which makes the control of the spray shape in different work condition not easily controllable.

Multi-hole injectors have been studied and adopted for gasoline direct injection to overcome the above mentioned problem. The development of this type of injectors exploited the know-how about multi-hole nozzles in diesel direct injection applications. The main difference between injectors for diesel and gasoline direct injection is that diesel injectors operate at much higher pressures since the fuel is injected in the compression stroke when the in-cylinder conditions are favorable for the auto-ignition of the fuel; injectors for gasoline direct injection application operate, in most of the cases, at pressures not higher than 250[bar].

The multi-hole injector consists of several fine openings, which are attached to the side of the injector tip. It is highly flexible and can be adjusted according to the

design requirements of the combustion system. The position and number of nozzle's holes, the direction of single fuel jets and the overall spray direction and cone angle are parameters that can be adjusted in the design phase of the injector. The holes are commonly placed on a periphery of a circle, in either symmetric or not symmetric pattern, but there is also the possibility of including centrally located holes in every design.



Figure 1.2: Multi-hole solenoid injector for GDI by Bosch GmbH

This study is based on 5-holes high-performance injectors used mainly for motor-sport applications. The experimental analysis is carried out on two different types of injectors; these two injectors present the same design, but differ in terms of fuel mass flow rate. The following CFD analysis considers the results obtained from experimental tests of these injectors in order to create an improved model for fuel injection in the *Quicksim* software. The details about the investigated injectors will be given in the next chapter about the experimental test campaign.

1.2 Engine future developments

The development of internal combustion engine as a complete system, but also the development of particular technologies applied to internal combustion engine, as, in this case, injection system, can be obtained by means of different tools that can be categorized into two main categories [6]:

- experimental tools: test bench and labor investigation
- theoretical tools: calculation and CFD simulation analysis

Each tool of these main categories differs in terms of application range, level of details, predictability, resource consumption, etc., so that at the end the spectrum of available development tools is very wide.

While experimental techniques are developing to capture combustion and emission characteristics of GDI engines, simulations of multi-dimensional computational fluid dynamics (CFD) modeling acts as a powerful predictive tool to complement the relevant analysis and studies. One of the advantages of simulations modeling approach with respect to experimental analysis is that it is more cost-effective when it comes to investigate engine processes across a wide range of operating conditions and various geometric configurations. The accuracy of numerical results depends on the models selected to represent the in-cylinder events of engine operating cycles, and to describe the chemical kinetics of fuels [7].

In the following, a small description of these tools will be given focusing on the subject of this thesis, which is fuel injection in gasoline direct injection engines.

1.2.1 Injection experimental analysis

Experimental investigation of injection events is aimed to characterize the spray, and describe the behavior of some quantities related to the spray as a function of the different injection conditions. The most important investigated quantities are [1]:

- Global spray characterization: geometry and spray targeting (focus on spray angles and penetration).
- Droplets characterization: size, diameter, distribution.
- Other spray-describing quantities: speed, vapor phase, temperature and density distributions.

Several optical spray diagnostic techniques have been developed. These techniques can be categorized mainly as *imaging* and *non-imaging* optical methods; the former type of tool deals with global spray characterization, while the latter allows the study of single droplets.

It is not in the interest of this work to analyse the different types of optical diagnostic techniques. The experimental investigation here developed and reported starts from high-resolution videos, recorded at the test rig, of injection events in a constant volume chamber with optical access. A tool able to analyse these videos and provide spray characterization quantities has been developed as first step of this thesis. The injection events have been reproduced under different conditions for injection pressure and chamber counter pressure in order to make observations and statements about the dependence of spray characteristic on injection conditions.

1.2.2 3D-CFD simulation

The three-dimensional simulation (3D-Computational-Fluid-Dynamics simulation) represents the most detailed and comprehensive approach to numerically investigate any fluid-dynamical problem. For this purpose the domain of interest is discretized into a computational grid, consisting of a multitude of finite volumes (up to millions of cells). The computational mesh serves as a framework for the local numerical solution of the discretized governing equations, which allow to calculate the reactive flow field. This is done on the basis of differential equations in dependence of time and three spatial coordinates. The time variable is also discretized, similarly to the spatial variables, into a sequence of small time intervals called time-steps, so that the solution of the flow field at time t_{n+1} is calculated from the known solution at time t_n .

The coupling of conservation equations for mass, momentum and energy with an equation of state enables a thorough description of fluid flows inside an engine. The complete derivation of these conservation equations is not reported, as it is not in the interest of this work. However a brief overview will be given in the following [5] [6].

The general form of a conservation equation of an extensive variable $F(t)$ can be written as follows (Euler formulation):

$$\frac{\partial f}{\partial t} + \text{div}\vec{\Phi}_f = s_f + c_f \quad (1.1)$$

where $f(\vec{x}, t) = dF/dV$ is the corresponding variable density of $F(t)$ in the volume element at the position \vec{x} . The conservation equation states that a change of the variable density $f(\vec{x}, t)$ can be caused by a flux $\vec{\Phi}_f \cdot \vec{n} dS$ through the surface of the volume element, due to convection or diffusion processes. The source terms s_f and c_f both describe changes of the conservation quantity, which can either be caused by local generation or reduction of the quantity inside the volume or globally by distant effects like gravitation or radiation.

From this equation, the conservation equations for mass, momentum, and energy can be derived.

- **Mass conservation equation** (continuity equation):

considering the mass m of the volume element as the extensive variable $F(t)$, the variable density is given by the mass density ρ , and the flux is given by the product of the local flow velocity \vec{v} and ρ . Furthermore, since the total mass does not change during the engine process, the source terms can be omitted ($s_f = 0$, $c_f = 0$). The conservation mass is described by the continuity equation

$$\frac{\partial \rho}{\partial t} + \text{div}(\rho\vec{v}) = 0 \quad (1.2)$$

In the case in which the distribution of mass fractions of the different species within the flow region is of interest ($w_i = m_i/m$), like in the case of fuel distribution in the combustion chamber, the corresponding mass density $\rho_i = \rho \cdot w_i$ is applied, and the local flow velocity is given by the sum of the average flow velocity \vec{v}_i and the diffusion rate \vec{V} ($\vec{v} = \vec{v}_i + \vec{V}$), which generates the mass flow \vec{J}_i of species i . Furthermore, the generation and reduction of individual species, due to chemical reactions, are expressed by means of molar mass M_i and molar formation rate ω_i . The resulting formulation of the conservation equation is:

$$\frac{\partial \rho_i w_i}{\partial t} + \text{div}(\rho w_i \vec{v}) + \text{div}(\vec{J}_i) = M_i \omega_i \quad (1.3)$$

- **Momentum conservation equation** (Navier-Stokes equation):

In the case of conservation of momentum, the terms in equation 1.1 can be substituted as follows. The variable density f is given by the momentum density $\rho \vec{v}$, the momentum flux is divided into a convective part $\rho \vec{v} \otimes \vec{v}$ and the second order stress tensor $\overline{\overline{P}} = p \overline{\overline{I}} + \overline{\overline{\Phi}}$, which describes a change in momentum due to pressure p and viscous effects expressed by means of the shear stress tensor $\overline{\overline{\Phi}}$. The term c_f takes into account the gravitation $\rho \vec{g}$.

$$\frac{\partial \rho v}{\partial t} + \text{div}(\rho \vec{v} \otimes \vec{v}) + \text{div}(\overline{\overline{\Phi}}) - \text{grad}(p) = \rho \vec{g} \quad (1.4)$$

- **Energy conservation equation:**

The conservation equation of energy can be derived in various forms. In the most general formulation the energy amount is composed of the internal energy u , the kinetic energy, the potential gravitational energy G and the heat of formation of the mixture h_f (chemical energy).

The total energy density is given by:

$$\rho e = \rho \left(u + \frac{1}{2} |\vec{v}|^2 + G + h_f \right) \quad (1.5)$$

The energy flow consists of a convective term $\rho e \vec{v}$, energy transport \vec{J}_q due to thermal conduction and an additional term $\overline{\overline{P}} \vec{v}$, which characterizes the change of energy due to pressure and friction forces. The source term c_f takes into account effect q_r of radiation or magnetic fields. Kinetic and gravitational energy can be neglected, and the equality $\rho h = \rho u + p$ can be applied.

The energy conservation equation becomes:

$$\frac{\partial \rho h}{\partial t} - \frac{\partial p}{\partial t} + \text{div}(\rho h \vec{v} + \vec{J}_q) + \overline{\overline{P}} : \text{grad}(\vec{v}) - \text{div}(p \vec{v}) = q_r \quad (1.6)$$

These set of equations build an equation system of $6 + N_i$ scalar equations for each finite volume, where N_i is the number of described species in the gas mixture. In order to close this system, several laws and models, mostly based on empirical formulations and mainly as a function of the physical properties (ρ , T , \vec{v} and w_i) are required. These laws or models are used to convert the physical problem into a mathematical formulation.

In an internal combustion engine application, it is necessary also to implement the calculation of turbulence of the flow. Different turbulence model approaches are available which can be classified according to their length and time scales. The most common are the Direct Numerical Simulation (DNS), which describe turbulence up to the smallest turbulent length scales and solves numerically the equations, the Large Eddy Simulations (LES), which are characterized still by highly refined computational meshes for the explicit determination of large eddies, and the Reynolds Averaged Navier Stokes (RANS) equations, which is the standard in engine flow fields simulation. RANS equations describe the turbulent flow completely by models, and an explicit numerical solution of the equation is omitted, resulting in a significant reduction of computational effort.

The range of application of 3D-CFD simulation is theoretically widespread, but the main issue is always the trade-off between accuracy of the simulation and computational time. In engine application it is necessary to limit the analyzed engine domain in order to save computational time, thus requiring a very precise definition of boundary conditions in order to obtain highly predictive and reliable simulations of complex thermo-fluid-dynamical phenomena.

However, an immediate integration into the engine development process is only conditionally reasonable and feasible, due of the very high processing and computing time as well as the limited informative value of extracted simulation domains with respect to the full engine behavior. Therefore, 3D-CFD simulations are more commonly deployed for research purposes or isolated (pre-) development tasks [5].

1.3 Objective of the Thesis

After this brief theoretical overview of the topics that will be dealt with, this last section of the introduction is dedicated to outline which are the main steps and the final goals of this thesis.

It is possible to divide the work in three main phases:

1. Experimental tests analysis.
2. 3D-CFD simulation of injection events in the same injection conditions of the

tests.

3. Exploit experimental results for the improvement of the injection model of the simulations.

1.3.1 Experimental tests analysis

The first phase is the analysis of the experimental tests of injection. This task is carried out through the creation of a tool which allows to analyse high-resolution videos coming from the test bench in order to obtain a characterization of the spray. With this tool is possible to study the development of the spray during the injection event, its kinematic and its geometry (especially spray angles and penetration). These results are then processed in order to show how injection conditions influence fuel spray development. A peculiar feature of this tool is that it has been designed to be used both for experimental data, but also for the analysis of the simulations' output. It is clear how this characteristic of the tool allows also to make comparisons between experiments and simulations with the final goal of validating the injection model adopted in CFD simulations.

The development, the features and the potential of this tool are described in details in the next chapter, where the obtained results of the analysis are also reported.

1.3.2 3D-CFD simulation of injection

The software used for the 3D-CFD simulations is *Quicksim*, whose features will be described in detail in Chapter 3.

3D-CFD simulations of injection have been done under the same injection conditions of the experiments, thus allowing a direct comparison between the two sets of results. The influence of the different injection initialization parameters on the simulation's output is investigated in order to define a set of criteria to chose the best combination of them, which provides a good reproduction of the results observed from the tests. At first these parameters are studied singularly, and afterwards their combined effects are analysed. The injection initialization parameters are the ones that define the properties of the injected fluid droplets from a thermodynamic (temperature, density, viscosity, heat of vaporization, saturation pressure, etc.) and kinematic (speed, spray targeting, diameter, etc.) point of view; they are characteristic of the adopted software, so they will be presented in the dedicated chapter of this thesis.

Even if these simulations are mainly aimed to verify the matching between experimental and simulation's results, an analysis of spray parameters that are not investigated experimentally is an essential point of this phase. In particular the Sauter Mean Diameter (SMD) and mass distributions of the droplets are analysed

to get a deeper understanding of the behavior of the injection phenomena, such as spray propagation, vapor phase development, and air/fuel mixture formation.

1.3.3 Improvements of 3D-CFD injection simulations

The final, and most important step of this work is the coupling of simulation and experiments. It is apparent that simulation and experiments can go hand in hand to provide the maximum understanding of the complex phenomena occurring, such as fuel injection, fuel/air mixture formation, and combustion. This is the most effective way to move towards what is the goal of this work: the improvements of 3D-CFD simulation of injectors, which means, from a wider perspective, an improvement of GDI engines simulation.

The approach followed in this phase is based on the concept of exploiting the experimental data to calibrate the simulations and reproduce the injection events with a better approximation. The definition of a calibration methodology have required several simulation runs, in which the injection initialization parameters have been modified according to the results of experimental tests' analysis.

During this procedure some criticalities have emerged, which are mainly related to the sensibility of the spray development to variation in injection conditions, and to the quality of the imaging tool used for the analysis of experimental tests. In order to overcome these criticalities, two main paths have been followed:

- Calibration of parameters which are not related to the experimental data investigated before, such as the SMD of initialization.
- Deeper insight in the models that are used by the CFD software to treat the spray initialization and development as, for example, vaporization, turbulence, or break-up models.

These actions lead to achieve a significant improvement in the comparison between experimental results and simulations, thus allowing to state that the developed methodology can be used in future analysis to set up 3D-CFD simulations of injection, which provide satisfactory results, without the need of possessing experimental data from the beginning.

In the chapters which deal with 3D-CFD simulation all these aspects are described in details, following step by step the development of this calibration methodology, and reporting the most relevant results, maintaining the focus on how the combined usage of experimental data and simulation technology is one of the key factor in future engine development.

Chapter 2

Experimental Tests Analysis

In this chapter the analysis of experimental tests of injection is reported. It starts with the acquisition of high-resolution videos of injection events in a test chamber with optical access at the test bench, and it continues with the analysis of these videos using an ad-hoc developed tool, which provides several output about the spray.

In the following, the nature, the purpose and the results of this analysis are described in details.

2.1 Experimental Set-up

The investigated experiments have been conducted under quiescent flow conditions in a constant volume test chamber with optical accesses which allow an high-resolution camera to record the injection events at a frame rate of 23000frame/s . The thermodynamic state inside the chamber can be modified in order to simulate different possible in-cylinder conditions of temperature and pressure during a real engine cycle. Nevertheless the tests have been conducted with variations only in injection and chamber pressure.

The injected spray is observed from two different points of view. Considering a reference system centered in the injector tip in which the Z axis correspond to the chamber axis, the points of view are:

- ZY plane
- ZX plane

Two types of injector are used for experimental tests. The two injectors are 5-holes high-performance injectors. The versatility of such injectors make them qualified for various applications, both for consumption (e.g. downsizing) and fun-to-drive

concepts (e.g. in combination with turbocharging) [9]. In this case, the two investigated configurations of these injectors present the same jet target points, but different angles and flow rate. In the following they will be referred to as injector of type *F* and injector of type *G*. The main characteristics are reported in table 2.1 and a graphical representation of the points listed in table 2.1 is reported in figure 2.1.

Jet Nr.	$x[mm]$	$y[mm]$	$z[mm]$	Flow Rate [%]
1	-0.50	0.00	30	0.200
2	3.00	-11.00	30	0.200
3	6.50	-18.00	30	0.200
4	6.50	18.00	30	0.200
5	3.00	11.00	30	0.200

(a) Spray jets target points

Type of injector	Flow rate @10[MPa]
<i>F</i>	656.5[g/min]
<i>G</i>	985.0[g/min]

(b) Injector flow rate

Table 2.1: Injectors characteristics

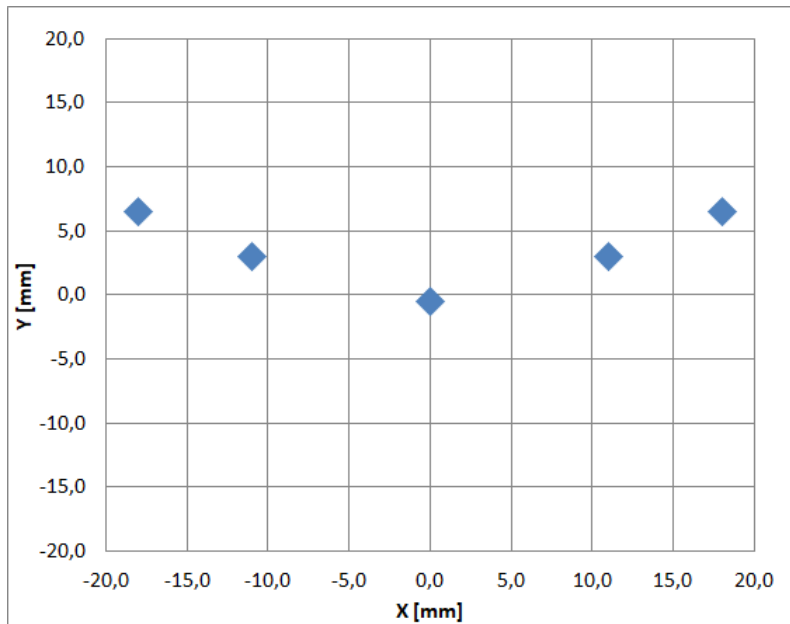


Figure 2.1: Injector target points

Several injection events are recorded, and the generated videos will be the input for the experimental investigation carried out as first phase of this work.

Table 2.2 represent a summary of the conducted tests. Note that the total number of produced videos is twice the number of tests because two different points of view (ZX and ZY planes) are considered.

Test Nr.	Type of injector	$P_{chamber}$ [bar]	$P_{injection}$ [bar]
1	<i>F</i>	1	100
2	<i>F</i>	1	200
3	<i>F</i>	5	100
4	<i>F</i>	5	200
5	<i>F</i>	10	100
6	<i>F</i>	10	200
7	<i>G</i>	1	100
8	<i>G</i>	1	200
9	<i>G</i>	5	100
10	<i>G</i>	5	200
11	<i>G</i>	10	100
12	<i>G</i>	10	200

Table 2.2: Tests summary

2.2 Procedure and Investigated Quantities

Investigation over injector spray features are ususally lead through a camera analyzing the following spray characteristics:

- Injection shape
- Spray penetration
- Particle size and speed distribution

The evaluation is based on the analysis of the different frames, with the final goal of a qualitative and quantitative assessment of the above mentioned jet characteristics. In order to do so, a Matlab tool has been developed. This imaging tool takes as only input the video recorded at the test bench, and it is able to provide both numerical and graphical output about the most important spray characteristics for every frame

of the video.

The development of this tool has been carried out considering its application in the overall analysis of the injector, thus not only allowing a faster experimental test analysis, but also providing numerical data about the injections that can be directly used to perform a faster calibration of the initialization parameter for 3D-CFD simulation of injection, resulting in an improvement of the simulation's accuracy. A simulation quality evaluation can be also performed exploiting a variant of this tool which takes as input the frames obtained from both experiments and simulation, and compares the two mentioned sets of images in order to verify their matching. This procedure have been exploited throughout all the analysis performed.

Moreover the potential of this tool is that it can be used for analysis of injection of different fluids, and, after an appropriate and fast calibration, it can be used for analysis of tests from different test chambers.

The final numerical output quantities of this analysis is the evolution in time of the following parameters:

- Spray axial penetration
- Spray vertical penetration
- Spray angle
- Spray exit speed

The different tests are exploited to make statements about the dependence of these output parameters on input injection conditions (injection pressure, chamber pressure) and type of injector (type F , type G).

2.2.1 Imaging Matlab Tool Description

The imaging tool used for experimental analysis has been developed in Matlab. The script is divided into two main sections, that must be run subsequently, and can be identified as:

- Video acquisition
- Frame analysis

The first section consists in the acquisition of the experimental video of an injection event and its subdivision into single frames, which are then stored. It is then up to the user to manually select which frames must be processed by the second section of the tool.



(a) 0.2[ms]ASOI

(b) 0.4[ms]ASOI

(c) 0.6[ms]ASOI

Figure 2.2: Example of acquired frames of experimental video using Matlab tool showing the evolution in time of the spray.

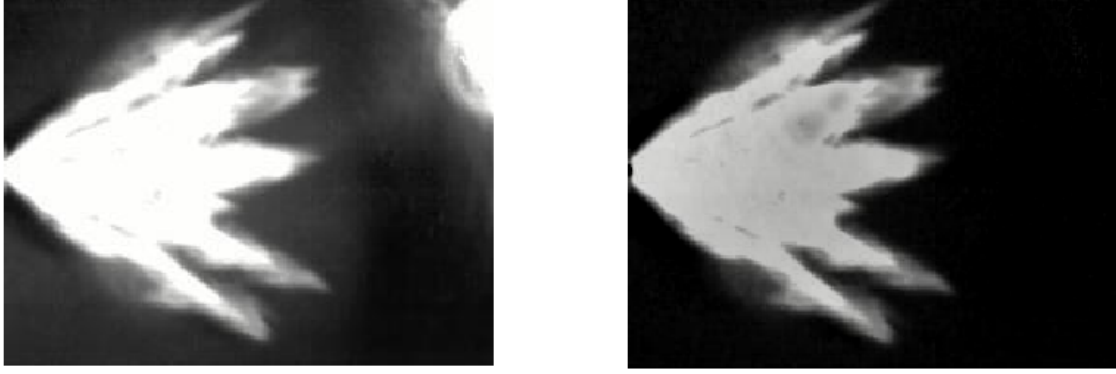
In figure 2.2 an example of frames captured from the injection video at different time instants is reported.

The spray analysis is based on the recognition by the software of the boundaries of the spray, and the subsequent parameters' evaluation. The recognition of the contour of the spray is made considering the different level of luminescence between the spray, which is bright, and the background, which is dark; in order to facilitate this process, each image is elaborated to eliminate light spots due to the design and lighting system of the test chamber, or the camera set-up. This image processing step allows to have completely black frames when the injection is not started yet, and white spray on black background when fuel is injected in the chamber, thus eliminating the probability for the software to identify redundant light spots as part of the studied jet. Figure 2.3 shows an example of this imaging phase, necessary before starting the analysis.

The last thing that must be done before starting the analysis of the frames is to correctly calibrate the conversion between lengths in pixels and millimeters, thus allowing to make correct measurements of the quantities related to the injection. This need represents the only constraint of this tool, as it is required the knowledge of a reference length inside the studied test chamber in order to evaluate the correct conversion factor.

The section of the tool dedicated to the analysis of the frames starts with the recognition of the boundaries of the spray for every time instant, and the evaluation of the above mentioned quantities related to the spray: axial penetration, vertical penetration, spray angle and exit speed.

In the following these parameters will be referred to as:



(a) Injection frame from test bench video

(b) Injection frame ready for analysis

Figure 2.3: Example of image processing of the injection video before the analysis

- Axial penetration $\rightarrow x$ or x_{max}
- Vertical penetration $\rightarrow y_{max}$ and y_{min} , indicating the penetration below and above the injector tip respectively
- Spray angle $\rightarrow \alpha_{max}$ and α_{min} , indicating the angles below and above the injector tip respectively
- Exit speed $\rightarrow v$

These data are stored, and further manipulations are made, especially concerning the spray angle analysis.

The spray angle is evaluated at first considering the points of maximum and minimum vertical penetration (y_{max} and y_{min} respectively). Anyway a double check is made considering the angles obtained at fixed axial distances from the injector tip (2.5[mm], 5[mm], 10[mm], 20[mm], 30[mm]) and calculating the mean between these values. This procedure should eliminate problems related to possible misleading values of penetration measured when the spray reaches the edges of the frame, or a strange deformation of the jet is present.

The spray angle is also taken as reference parameter to conduct a preliminary investigation about the variation and coherence of the spray's shape throughout the injection period. Once the data of the spray angle trend in time are available, a statistical analysis is performed in order to observe if, how, and how much the spray modifies its shape during the injection. The statistic parameter used for this goal is the *Coefficient of Variation*, in short *CV*, which is a standardized measure of dispersion of a probability distribution or frequency distribution. This coefficient is an adimensional parameter which expresses the *Standard Deviation* in terms of

percentage, and it is defined as:

$$CV = \sigma/|\mu| \quad (2.1)$$

The CV varies in the range $0 \leq CV \leq 1$.

In this context this parameter is used to have a measure of the dispersion of the spray angle measurements, thus allowing to make statements about the variation in time of the shape of the spray. In general the smaller the *Coefficient of Variation*, the less dispersed are the data. As it is shown in the section concerning the results of the analysis, in all the investigated experimental tests the tool has shown small values of dispersion of the spray angle values, which means that on one hand the jet maintains its shape throughout the whole injection, and on the other end the tool provide reliable data about the angles.

The developed Matlab tool provides, alongside numerical stored data output, some graphical output, which manage to give the user a more immediate description of the injection development in time. In the following these additional output are listed, and some examples are reported.

Each injection frame is analysed and a summary of its most important properties is summarized as shown in figure 2.4.

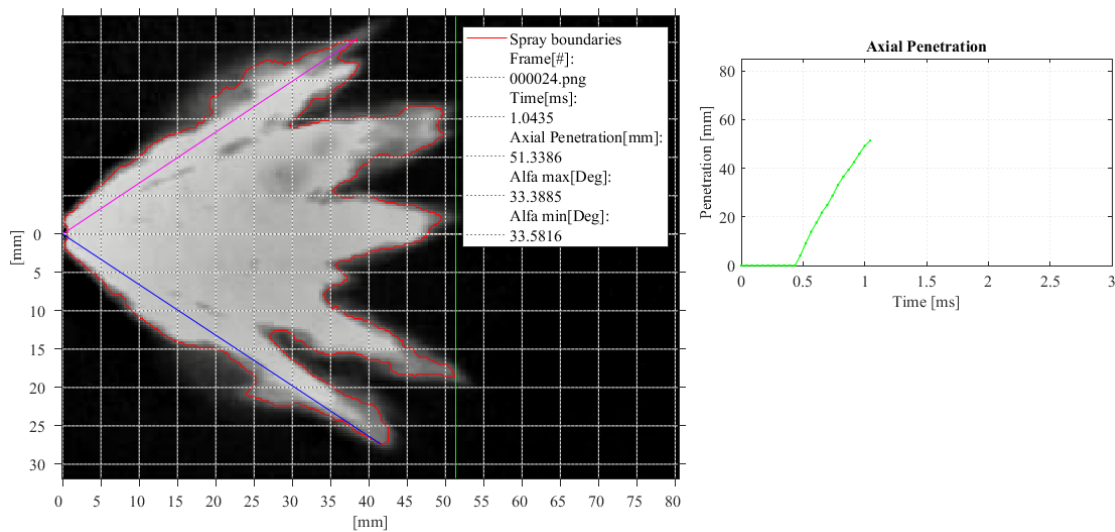


Figure 2.4: Analysed frame example

In this kind of image it is possible to observe:

- Spray contour (red)
- Maximum axial penetration (green)

- Spray angles (blue and magenta)
- Legend box containing time instant and the corresponding numerical values of the above mentioned quantities
- Live axial penetration curve

The penetration curve has been placed next to the video frame in order to let the user have an idea of the development of the spray during injection instant by instant. All the images obtained from processed frames are also used to create an output video, whose intent is to reproduce the input video coming from the test bench showing the jet's properties at the same time.

An overall representation of the data extrapolated from the experimental tests is provided graphically by plots such as the one shown in figure 2.5. Here all the results obtained from the analysis of an experimental test are summarized. This kind of representation will be used also later for the comparison between experimental results and simulation; the comparison's graph present the same layout, but two sets of curves are present, thus allowing a very quick preliminary evaluation of the quality of the simulation.

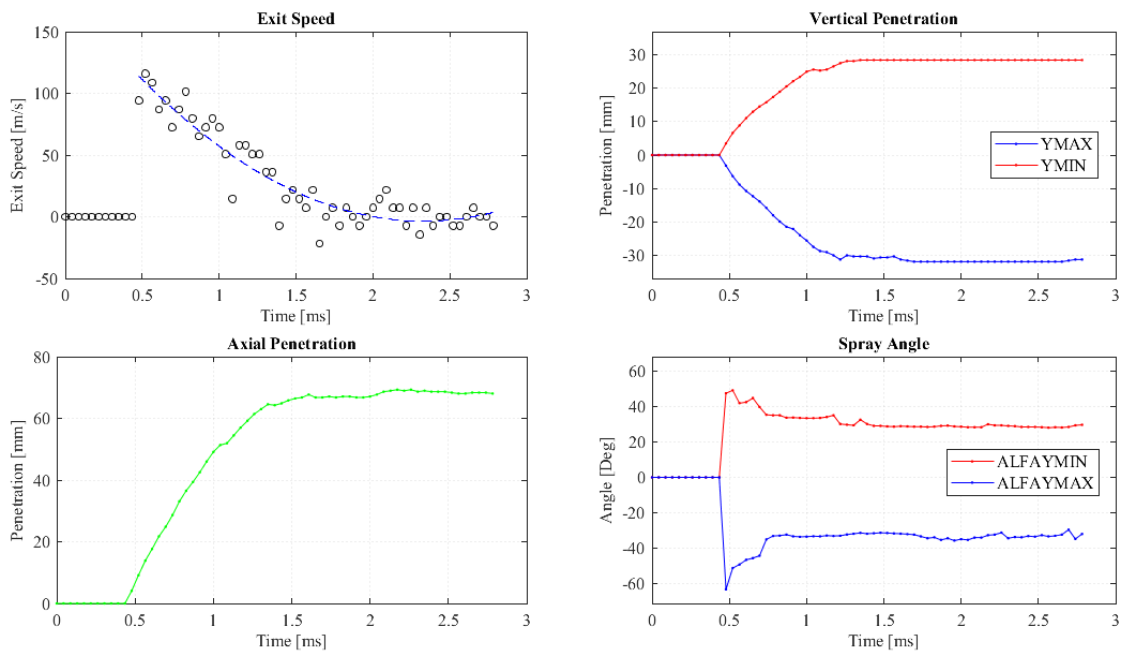
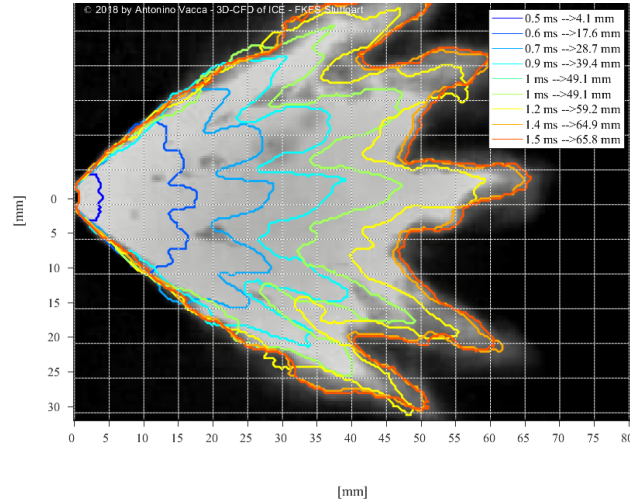


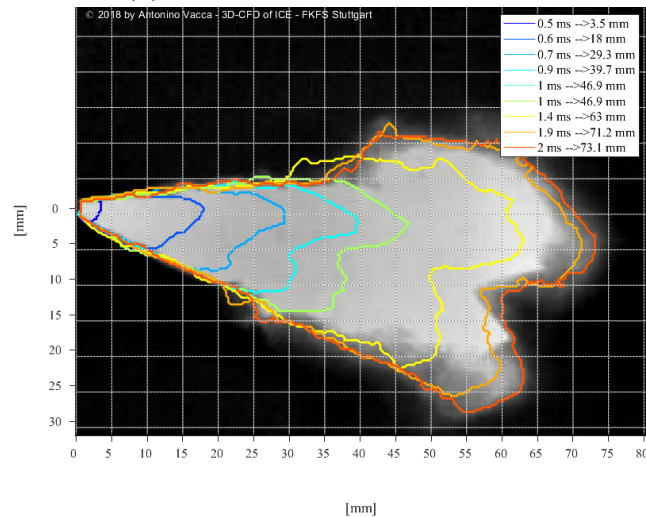
Figure 2.5: Analysis results plot

Last graphical output provided by the tool is a representation of the propagation of the spray in time, by means of its contours, with particular focus on the first phase

of injection. Figure 2.6 is an example of this kind of output. In this figure it is represented the same spray, but from the two investigated points of view.



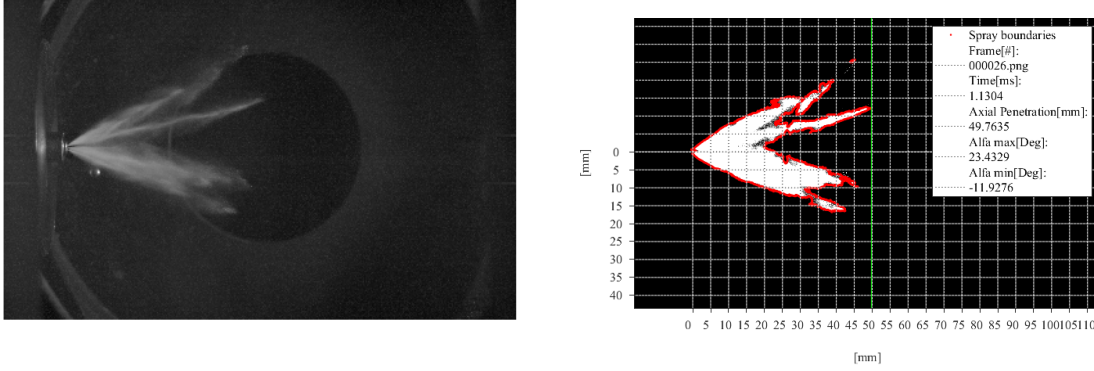
(a) Spray propagation in ZY plane



(b) Spray propagation in ZX plane

Figure 2.6: Spray propagation

This tool's versatility has been tested in order to prove the possibility of using it when analysing tests coming from different test chambers or using different injected fluid. In the following some examples of these adaptation tests are reported. Figure 2.7 shows the original frame of a injection test in a different tests chamber than before, and the injected fluid in this case is water and not gasoline.



(a) Original frame

(b) Analysed frame

Figure 2.7: Example of adaptation of the tool for the analysis of injection in different test chamber (water injection)

2.3 Analysis Results

This section is aimed to be a report of the experimental tests analysis results, with focus on the dependence of calculated spray characteristics on the injection conditions (injection pressure P_r and chamber pressure P_k) and on the type of injector. The two types of investigated injectors differ in spray target angles and fuel flow rate (see tale 2.1b at page 12).

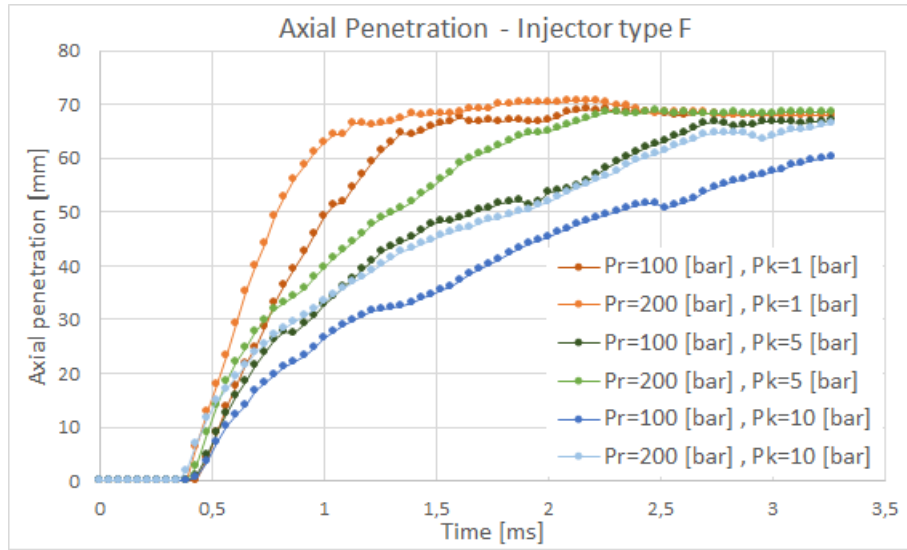
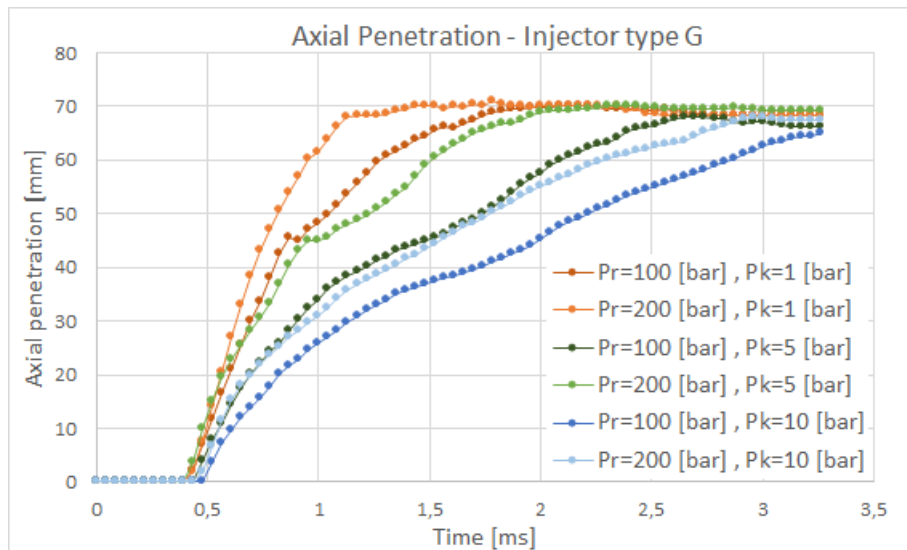
After having studied each test chamber's video with the tool just described, each output quantity is investigated in detail before assessing some final conclusions.

2.3.1 Spray Axial Penetration

The penetration curves registered from all the analysed tests are summarized in graphs which allows to read the behavior of them as a function of injection pressure and chamber pressure. Figure 2.8 and figure 2.9 report the results obtained for both injectors from ZY plane point of view.

Qualitatively it is possible to observe two main trends related to the axial penetration of the spray: increasing rail pressure and/or decreasing chamber pressure cause an increase in the punctual values of axial penetration, and also a faster ascent towards its maximum value. Between the two pressure conditions, chamber pressure P_k seems to be of greater influence on the final result, especially when moving from $P_k = 1[bar]$ to $P_k = 5[bar]$.

Injector F and injector G present a similar behavior in terms of trend of the penetration curves, but also from a numerical point of view. The only visible difference between the penetration curves is that sprays produced by the injector of type G

Figure 2.8: Spray Axial Penetration - Injector type F Figure 2.9: Spray Axial Penetration - Injector type G

present maximum values of penetration very close, regardless of the pressure conditions, while it is possible to observe a larger difference between maximum values of penetration for injections of the injector of type F . Considering one particular case of test conditions ($P_r = 200[\text{bar}]$ and $P_k = 5[\text{bar}]$), the comparison between the two injectors is shown in figure 2.10.

Note that in the case of penetration calculation, only one point of view is taken into account. This is due to the fact that the images from different points of view show

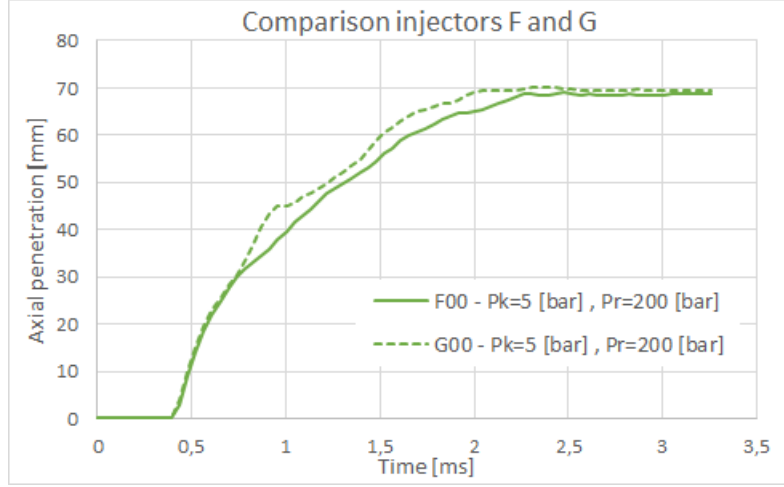


Figure 2.10: Comparison of spray axial penetration between injectors of type F and G in the case of $P_r = 200[\text{bar}]$ and $P_k = 5[\text{bar}]$

the same spray, thus should present the same penetration. Although there is the possibility of detecting errors that depend on the recording instrumentation used in the two planes. The calibration of the measurement scale is carried out in correspondence of the injector axis, and in the case of sprays with wide opening angle, this can lead to different registered levels of penetration depending on the viewing direction.

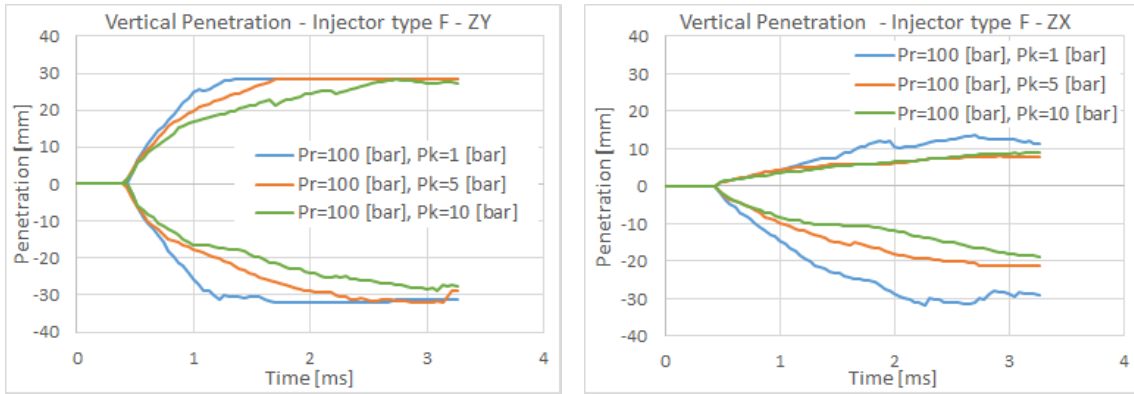
2.3.2 Spray Vertical Penetration

Vertical penetration is intended to be the width of the jet, the coordinate of the edges in y direction in the ZY plane and x direction in the ZX plane. In these measurements a crucial role is played by the limited dimensions of the window recorded at the test chamber. When the spray reaches the edges of the frame, no further considerations can be made about its development in that direction.

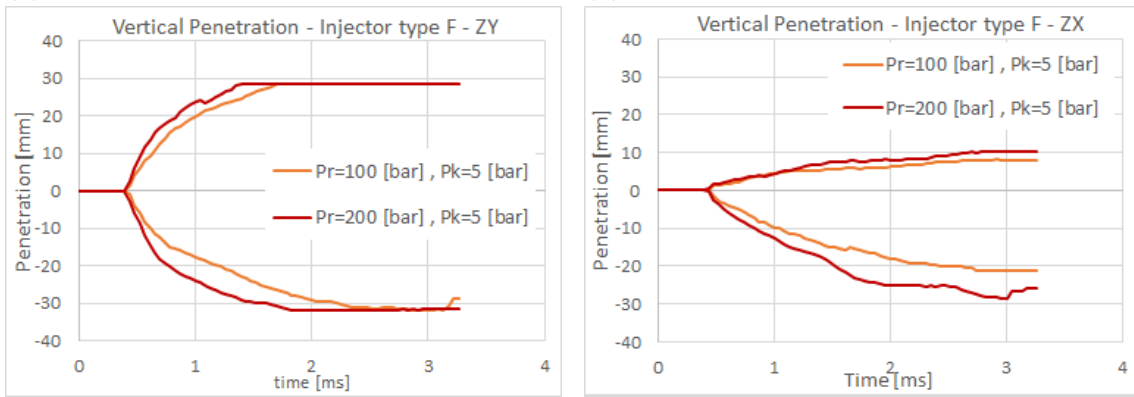
As expected, also these analysis has revealed the same trends observed for the spray axial penetration: penetration reaches higher values, and increases faster whenever rail pressure increases and/or chamber pressure decreases. Results are reported only for injector of type F in figure 2.11, where vertical penetration curves are shown as a function of injection pressure for constant chamber pressure, and viceversa.

The sprays show a certain asymmetry with respect to the injector's axis, especially in the ZX plane.

The analysis of vertical penetration in the two investigated directions, and the analysis of spray angle provide the quantities necessary for the description of the overall shape of the spray.



(a) ZY - Vertical penetration function of P_k (b) ZX - Vertical penetration function of P_k



(c) ZY - Vertical penetration function of P_r (d) ZX - Vertical penetration function of P_r

Figure 2.11: Spray vertical penetration for injector of type F as a function of Injection pressure and Chamber pressure

The obtained results show that the two injectors produce a spray with very similar shape, especially in the ZY plane. In the other direction the injector of type G produces a wider spray with respect to injector of type F , and both present really strong asymmetric shape. In figure 2.12 the comparison of the results for the two injectors, in the specific case of $P_r = 200[bar]$ and $P_k = 5[bar]$, is reported.

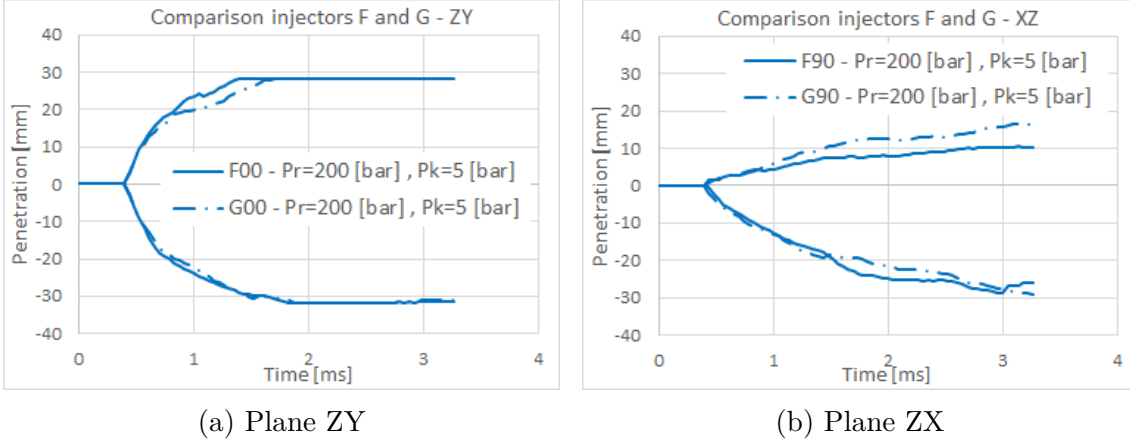


Figure 2.12: Comparison of spray vertical penetration between injectors of type F and G in the case of $P_r = 200[\text{bar}]$ and $P_k = 5[\text{bar}]$

2.3.3 Spray Angle

Among all the performed analysis, the spray angle is always characterized by a particular distribution in time, with an initial peak, followed by a fast transient phase towards an almost constant value of angle which is maintained for the rest of the injection.

The spray angle seems not to be highly affected by the variations in injection pressure or chamber pressure, with punctual differences not greater than 5° . The only effects observable from the results are the reduction in the initial peak value of the angle as injection pressure increases and/or chamber pressure decreases, and slightly wider spray in the case on injector G with respect to injector F , as expected. The spray angle results are reported in figure 2.13 for the injector of type F , while the results for the other type of injector are omitted since the behavior is almost equal. Only the difference between the two in a particular case ($P_r = 200[\text{bar}]$ and $P_k = 5[\text{bar}]$) is reported in figure 2.14.

As mentioned before, vertical penetration and spray angle, especially the latter since vertical penetration measurements could present unprecisenesses when the spray reaches the image's edges, are capable of providing information about the shape development of the spray in time. This point is further investigated by means of a statistical analysis on the dispersion of spray angle's values throughout the injection duration, in order to describe how and how much the shape of the spray changes in time. A stable spray should not vary significantly its shape in time, especially in the case of tests in a constant volume chamber where in-cylinder motions are not reproduced.

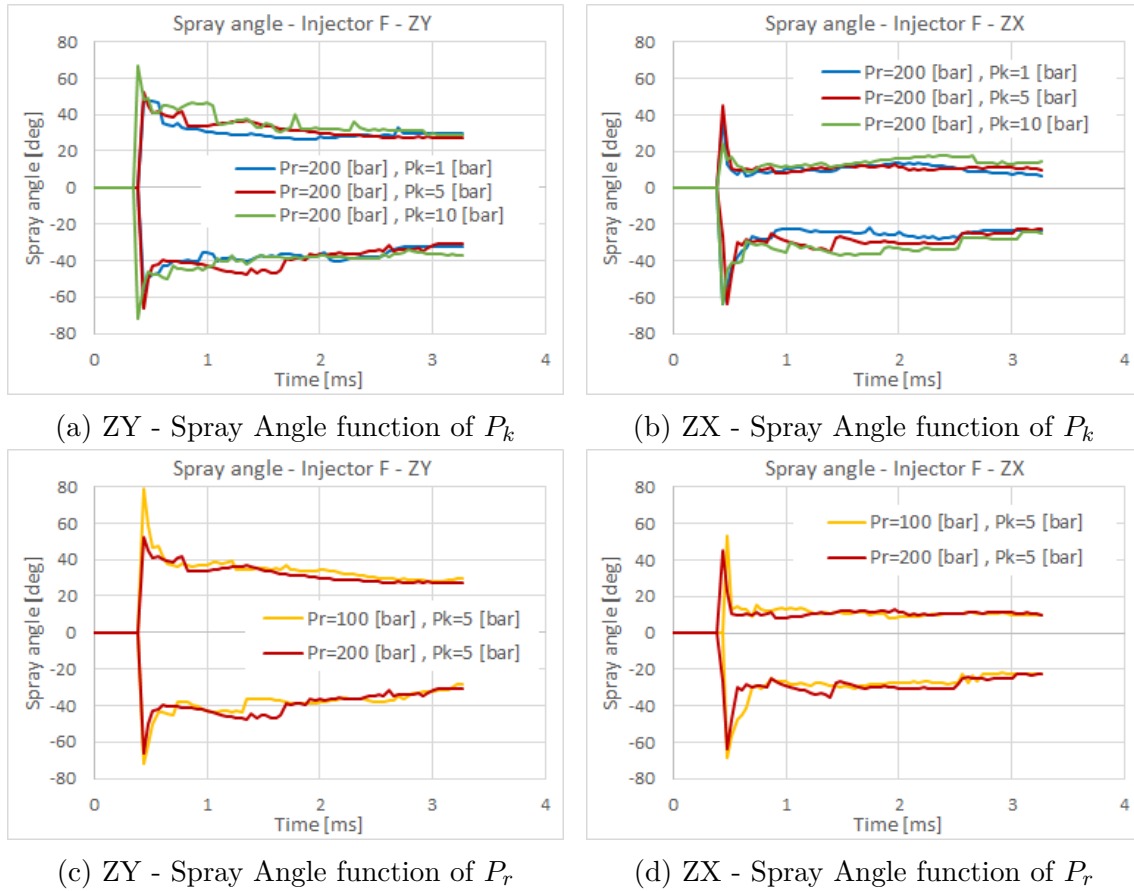


Figure 2.13: Spray Angle for injector of type F as a function of Injection pressure and Chamber pressure

The statistical instrument used to perform this evaluation is the *Coefficient of Variation* or *CV*; the calculated values of this parameter for the different tests are reported in figure 2.15.

The graph shows that almost every test show a variation of the spray angle during the injection lower than 30 %, thus, considering that also the initial angle values in the peak are subject of the calculation, demonstrating a good coherence of the jet in time. The spray shows higher variability of its shape in the ZX plane, where also the largest differences between the two injectors' behavior are present.

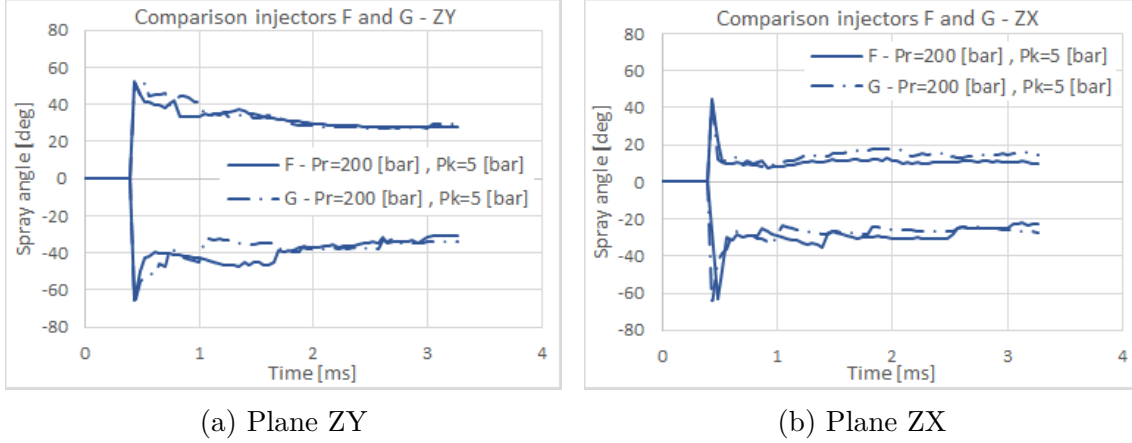


Figure 2.14: Comparison of spray angle between injectors of type F and G in the case of $P_r = 200[bar]$ and $P_k = 5[bar]$

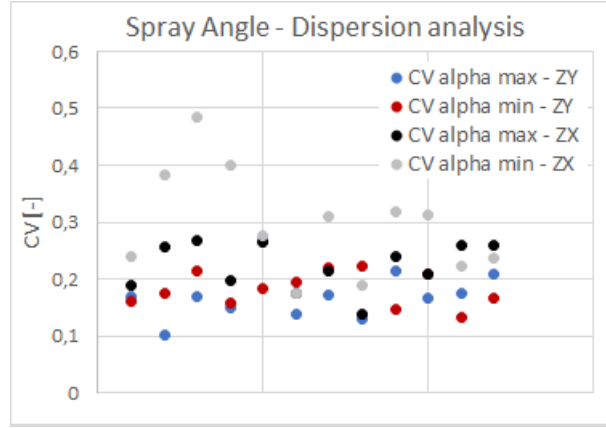


Figure 2.15: Spray angle dispersion analysis - CV

2.3.4 Spray Speed

The spray speed is evaluated as the derivative of the penetration:

$$v = \frac{dx}{dt} \quad (2.2)$$

where for each time step, the corresponding variation in axial penetration is considered.

After having evaluated the punctual values of speed, best fitting curves have been found and plotted to compare the different curves under different injection conditions.

For equal chamber pressure level, an increase in injection pressure level causes a

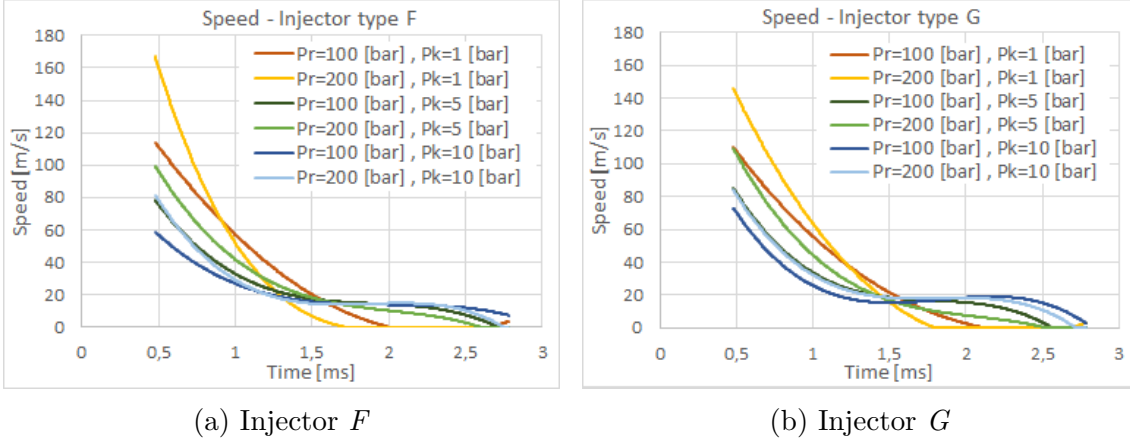


Figure 2.16: Spray Speed

significant increase in jet speed (up to 30%). This effect reduces as the chamber pressure level increases, in fact the maximum difference in speed between the tests at $P_r = 100$ [bar] and $P_r = 200$ [bar] is obtained for the lowest value of P_k . Initial high values of speed are followed by a steep slow down due to the fact that the spray is at its maximum axial penetration, or close to it, and the rate of penetration increment is very slow.

The graphs in figure 2.16 show also that the speed curves of the two types of injector have the same trend, with injector G having higher initial values of speed for high value of chamber pressure.

Spray speed is one of the fundamental parameter for the next step of this work, as it will be exploited to calibrate the initialization of the injection parameters in the 3D-CFD simulations of injection. In the next chapters the role of this parameter will be explained and analysed in detail.

2.3.5 Conclusions

In the following table 2.3 the most relevant considerations about the dependance of spray characteristics on injection conditions are summarized.

Furthermore additional considerations about the difference between the two injectors are made based on the observation of experimental tests videos. From spray images (both taken from tests under the same injection conditions) displayed in figure 2.17 it is possible to notice another difference between the two injectors. Figure 2.17a shows a spray produced by injector F , in which it is observable how the spray is characterized by a core very bright, indicating a large presence of liquid fuel, around which the spray is less bright and the contour is irregular, indicating

Parameter	Influence of injection conditions	Injectors comparison
Axial penetration x	$P_r \uparrow, P_k \downarrow \Rightarrow x \uparrow$ and higher increase rate	Curves with the same trend and similar final values
Vertical penetration y	$P_r \uparrow, P_k \downarrow \Rightarrow y_{max}$ reached faster Asymmetric spray in both views	Injector G produces wider sprays
Spray angle α	Variations of α_{min} or α_{max} lower than 5° for variations of P_k or P_r $P_r \downarrow, P_k \uparrow \Rightarrow$ initial peak \downarrow Spray's shape does not change significantly during injection (higher variability in ZX plane)	Injector G produces wider sprays
Speed v	$P_r \uparrow, P_k \downarrow \Rightarrow v \uparrow$ at the beginning of injection Effect of P_r lower as P_k increases	Curves with the same trend For high values of P_k injector G produces faster jets

Table 2.3: Summary of experimental tests analysis results

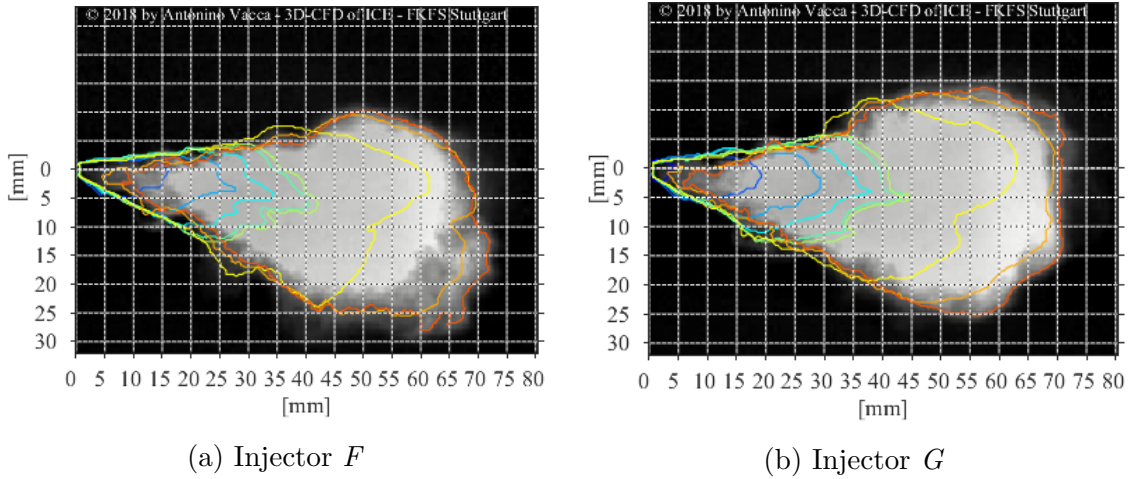


Figure 2.17: Example of spray propagation for the two types of injector - ZX plane

that in this region some fuel is vaporizing. These characteristics are far less visible in the case of injector G in figure 2.17b. The conclusion about these observations

could be that spray produced by injector F faces earlier vaporization with respect to spray produced by injector G . This peculiarity could be exploited in the injector choice when, for example, there are restrictions due to the chamber geometry or dimensions which imply constraints in terms of vaporization time.

Chapter 3

3D-CFD Simulation of Injection - Software

The next chapters are dedicated to the study of 3D-CFD simulation of injection, with focus on the modeling of injection for simulations, and on finding a suitable methodology able to improve the quality of injection simulation. This task is of particular importance not only in the design of injectors' geometry and injection strategies, but also in the wider context of full-engine simulation development. In fact, a well targeted injection of the fuel in sufficient quantity and at the right time has a decisive influence on the subsequent processes of ignition, combustion and pollutant formation. Full-engine simulations over several successive cycles enable a holistic analysis of the flow field and thus reliable and predictive statements on development-relevant questions [5].

All 3D-CFD simulations in this work have been performed using the tool *QuickSim*, developed at FKFS (Forschungsinstitut für Kraftfahrwesen und Fahrzeugmotoren Stuttgart) and IVK (Institut für Verbrennungsmotoren und Kraftfahrwesen) of the University of Stuttgart, which introduced a new concept in the simulation of internal combustion engines that aims to increase the relevance and reliance of the 3D-CFD simulation in the engine development process.

3.1 3D-CFD software QuickSim

The development of *QuickSim* was driven by the demand for a predictive and reliable 3D-CFD tool, which can be efficiently utilized within an internal combustion engine development process. There are several reasons for which an application of 3D-CFD simulations seems not suitable for industrial approaches, that exceed the pure research purpose. The main concerns are related to the extensive time demand of a 3D-CFD analysis of engine concepts, both in terms of CPU-time required

for the execution of simulations, and time required for the setup, calibration, and post-processing evaluations. Furthermore calculation models, mesh structure and boundary conditions may be an issue, since incorrect mathematical description of physical phenomena could lead to low level of reliability and predictability of calculations.

The purpose of *QuickSim* is to overcome these limitations in order to provide financial and temporal benefits and to enable comprehensive studies and a holistic virtual development of internal combustion engines. The main features of this tool are aligned with its purpose, and are largely discussed in [6]. Here a short description of *QuickSim* features is reported.

- Fast analysis: an application dependent reduction in the number of cells (from more than 1000000 to approximately 50000), alongside specifically ICE-adapted models, allows a significant reduction in the number of equations to be solved, thus resulting in an overall decrease of CPU-time up to a factor 100 without sacrificing results accuracy. Application-oriented modifications of the physical models can lead to a loss in general thermodynamic validity, but they are justified for the purpose of CPU-time reduction in the virtual engine development. A certain level of trade-off is acceptable, e.g. resigning detailed chemical reaction kinetics, while maintaining the necessary thermodynamic accuracy of the fuel heat release rate and wall heat transfer [5]. This feature allow *QuickSim* to rapidly analyse different operating characteristics, engine geometries, and control strategies.
- Full-engine 3D-CFD simulation: *QuickSim*'s time-savings in calculations allow to perform simulations of the entire engine domain, also for more than one operating cycle. For this reason *QuickSim* can be used in the engine development process starting even before the prototyping phase. There are no restrictions in terms of engine design, ignition type, fuel type, or operating strategy.
- Reliability of the results: the simulations performed by *QuickSim* produce reliable results, and are characterized by an high-degree of predictive capabilities. Furthermore the software provides output data in such a way that objective concept decisions can be made, and comparison with other simulations and experimental tests can be done.

The approach of *QuickSim* to the modeling of injector and injection strategy is based on an high level of flexibility in the definition of geometry, position, and type of injector. Although the initialization parameters, which include initial droplet characteristics such as velocity or diameter, need to be estimated for varying injection conditions, i.e. injection pressure, temperature, etc., in the case in which no reference data are available.

3.2 Fuel Injection Modeling in QuickSim

In order to understand the purpose and the methodology followed in this analysis, an overview on how the injection simulation is modeled in *QuickSim* will be given in the following, including how fuel properties, spray atomization processes, and the numerical injection definition influence the spray development and the mixture formation.

The analysis are carried out using gasoline as fuel, so here only liquid fuel properties and injection are described.

The fuel properties considered to describe the breakup and evaporation behavior of liquid fuel are the density ρ , viscosity η , surface tension σ , specific heat capacity c_p , heat of vaporization h_v , saturation pressure p_s and boiling temperature T_b . All these quantities, with the exception of the boiling temperature, are highly temperature and pressure dependent, but the pressure dependency can be generally neglected.

The injector is modeled by a coordinate system describing its mounting position, with origin in the point in which the injector should be placed, and z -axis oriented as the injector middle axis, directed towards the combustion chamber. Simplified variations in the geometry of the chamber are present only if the injector tip is significantly pushed inside the chamber.

The geometry of the injector is modeled on the basis of four characteristics spray angles, which are able to define the direction of the spray jets, in case of multi-hole injectors, the jet width, and an additional parameter describing the spray of hollow-cone injectors. The combination of these parameters allows to define the desired injector geometry in accordance to the spray targeting provided by the injector manufacturer. In the following these parameters are described and shown in figure 3.1. The direction of the jets is defined by means of spherical coordinates which define the direction of the jet middle axis: *zenit angle*, or polar angle, $\theta \in \{0,180\}$ describes the radial distance from the injector middle axis, and *azimuth angle* $\phi \in \{-180,180\}$ describes the jet orientation starting from the reference direction given by x -axis. The jet width is defined by means of angle α . For hollow-cone injectors the jet middle axis coincides with the injector middle axis z , thus *zenith* and *azimuth* angles are equal zero. Hollow-cone sprays requires an additional angle γ , since the angle α corresponds to half of the spray cone angle ϵ ($\gamma \leq \alpha$).

Another fundamental point in the injecton simulation with *QuickSim* is the initialization of the liquid fuel. In compliance with the purpose of the software to reduce computational time of the simulation, the concept of parcels is introduced according to the "Lagrangian Discrete Droplet Method". A parcel is defied as a group of a defined number of non-interacting droplets, which have identical physical properties. This approach allows to inject only a number of parcels large enough to

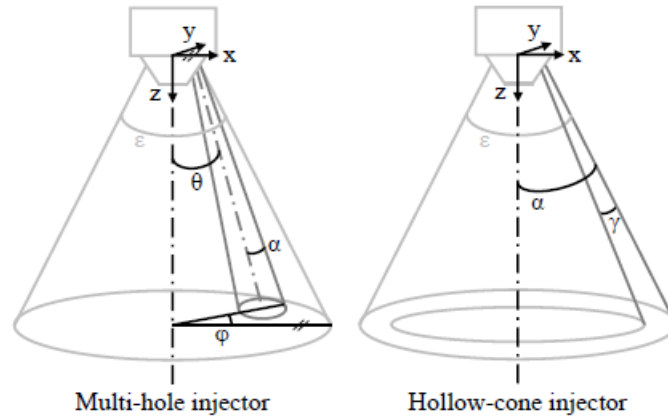


Figure 3.1: Spray angle definition

obtain sufficiently accurate representation of the spray, without the need of initialize each fuel droplet. For the sake of simplicity, droplets and parcels will be referred to as droplets.

Each liquid fuel droplet is provided with initial values for position, size, velocity, direction of movement and temperature, and it is introduced in the chamber in a spacial initialization domain given by a limited conical spray region near the injector orifice. This region is limited by angles α and γ , and by two values of axial distance from the injector tip L_{min} and L_{max} , as shown in figure 3.2.

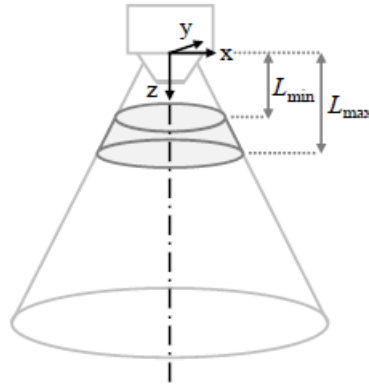


Figure 3.2: Definition of droplets initialization region

The consequence of this approach in the initialization of injected liquid fuel is that neither the injector internal flow, nor the droplet primary break-up are directly calculated by the software. The effort is concentrated in the definition of the individual droplet properties that have influence on the secondary break-up, and the

phase exchange process for mass, momentum, and energy, according to the standard Euler-Lagrange formulation of multi-phase flow.

Apart from the definition of the injector and spray geometries, other three parameters are fundamental to the injection simulation:

- Mass flow rate: it can be experimentally determined, or calculated by

$$\dot{m} = \frac{dm}{dt} = \rho \cdot v \cdot A \text{ [mg/s]} \quad (3.1)$$

where ρ is the fuel density, v is the flow speed, and A is the cross-section of the injector orifice. The value of mass flow rate can be adapted to pressure conditions by means of the Bernoulli equation.

- Sauter Mean Diameter (SMD): parameter which describes the droplet size distribution within the spray. It is defined as the diameter of the averaged volume-to-surface ration of all injected droplets. It can be measured with optical techniques such as PDA (Phase Doppler Analyzer), or it has to be estimated according to injector geometry and injection conditions. The initial value of SMD for the droplets is statistically determined using a Rosin-Rammler distribution, in order to have a significant reproduction of the actual droplets size spectrum of a spray.

$$N = 1 - e^{-\frac{D^q p}{s^q}} \quad (3.2)$$

where p , q and s are characteristic parameters of the distribution.

- Injection velocity: it is the initial velocity of each droplet. It can be determined experimentally, or calculated under the assumption of ideal flow (incompressible fluid, no friction)

$$v = \sqrt{\frac{2 \cdot \Delta p}{\rho}} \text{ [m/s]} \quad (3.3)$$

where Δp is the pressure differential between the injection pressure and the pressure in the combustion chamber.

3.2.1 Spray atomization models

The last topic to conclude the description of the fuel injection modeling with *QuickSim* is the description of how the software deals with spray breakup and evaporation. The breakup of the droplets is a fundamental phase in the spray atomization process, which is schematically reported in figure 3.3, and it is divided into primary and secondary breakup, which depend mainly on discharge velocity of the liquid jet,

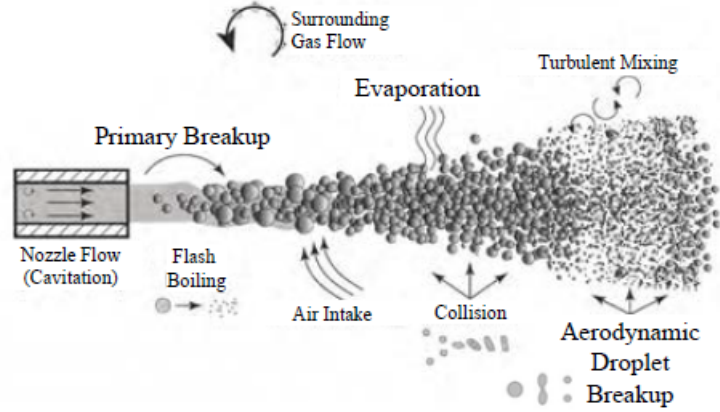


Figure 3.3: Spray atomization mechanisms [5]

and on aerodynamic forces affecting the jet respectively.

Primary and secondary breakup can be described exploiting the following adimensional quantities:

- Weber number:

$$We = \frac{\rho_g \cdot d_D \cdot v_{rel}^2}{\sigma_f} \quad (3.4)$$

which is the ration between inertia forces of a fuel droplet and its surface tension.

- Reynolds number:

$$Re = \frac{\rho_f \cdot d_D \cdot v_{rel}}{\eta_f} \quad (3.5)$$

which is the ration between inertia and viscous forces of the fuel droplet.

- Ohnesorge number:

$$Oh = \frac{\eta_f}{\sqrt{\sigma_f \cdot \rho_f \cdot d_D}} = \frac{\sqrt{We}}{Re} \quad (3.6)$$

which is function of surface tension and dynamic viscosity of the fluid.

Primary droplet breakup will not be discussed further, since is not directly included in *QuickSim*, although it is necessary to focus on the secondary breakup models. In fact, a correct calibration of the secondary breakup parameters could result in a more accurate simulation, especially in case of varying pressure and temperature conditions inside the chamber, which have influence of the spray penetration. If a droplet is exposed to a gas flow, significant deformation starts at a Weber number

of unity. Above a certain value of the Weber number, the droplet deformation leads to breakup [19]. This fact leads to classify different breakup mechanism according to characteristic values of Weber number. A detailed classification of these breakup mechanisms can be found in [21]. Several breakup models are implemented in STAR-CD and therefore in *QuickSim*, each one of them provide different models for the onset of droplets instability due to the interaction between the fuel droplet and the surrounding environment. Moreover the different models are characterized by different expression of the rate at which the droplet diameter decreases in time up to a stable diameter (dependent on breakup model), and its associated characteristic time. The rate of reduction of the droplet diameter is usually indicated as:

$$\frac{dd_D}{dt} = -\frac{d_D - d_{D,stable}}{\tau} \quad (3.7)$$

For example, the standard model adopted by STAR-CD is the Reitz-Diwakar model, which differs between two types of secondary breakup [8]: Bag breakup and Stripping breakup.

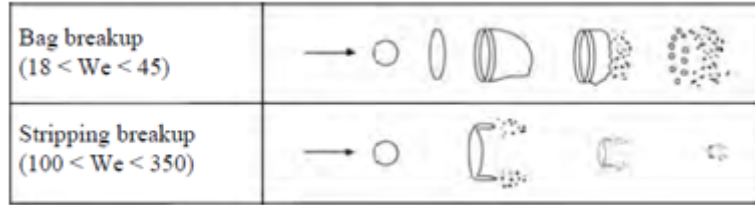


Figure 3.4: Reitz-Diwakar breakup mechanisms

- Bag breakup: non-uniform pressure field surrounding the droplet causes it to expand. When the applied forces overcome the surface tension of the droplet, it disintegrate. Instability is determined by a critical value od Weber number.

$$We = \frac{\rho|u - u_D|^2 d_D}{2\sigma_D} \geq C_{b1} \quad (3.8)$$

where C_{b1} is an empirical coefficient usually set $C_{b1} = 6$. The droplet size which satisfy the previous equation is the stable droplet size. The associated characteristic time is

$$\tau = \frac{C_{b2}\rho_d^{1/2} d_D^{3/2}}{4\sigma_D^{1/2}} \quad (3.9)$$

in which $C_{b2} \approx \pi$.

- Stripping breakup: the droplet breakup is caused by constant detachment or stripping of liquid from the droplet surface. The condition for the onset of instability is given by the following inequality

$$\frac{We}{\sqrt{Re_D}} \geq C_{s1} \quad (3.10)$$

where Re_D is the droplet Reynolds number and C_{s1} is a coefficient with default value of 0.5. The characteristic time scale is

$$\tau = \frac{C_{s2} \rho_D^2}{2 \rho} \frac{d_D}{|u - u_D|} \quad (3.11)$$

where the adjustable coefficient C_{s2} can assume value between 2 and 20.

Secondary breakup mechanisms cause a reduction in the dimensions of the droplets which lead to an increase in the specific fuel surface and in the rate of the evaporation process of the liquid which continuously changes into gaseous state according to the ambient temperature and pressure conditions. Evaporation process is strongly influenced by the fuel properties, and the gradient of pressure and velocity between the droplets and the surrounding gas.

The software models the exchange processes (mass transfer and heat transfer are the most relevant) by means of the basic conservation laws, represented by the equations of mass, momentum, and energy shown in Chapter 1. *QuickSim* also provides a model of evaporation which can take into account the effects of flash boiling.

3.3 Performed Injection Simulations

The goal of the set of performed 3D-CFD simulations is to validate the fuel injection model of the software, and try to improve its quality exploiting the data obtained by the experimental analysis. In order to do so, the simulations settings must reproduce the experimental tests conditions, in terms of injection conditions and duration, fuel properties, and spray targeting.

The chamber model used for the simulations is a faithful reproduction of the actual test chamber in which the experimental tests have been performed. As mentioned before, the peculiarity of the models used in *QuickSim* is that the injector is not physically present in the structural mesh, but it is obtained as a coordinate system properly positioned. In this case the injector is centrally mounted and the axis of the injector coincide with the axis of the chamber. Furthermore the mesh has been refined according to the particular application, with small cells in the central part of the chamber, where the fuel is injected. The model of the combustion chamber

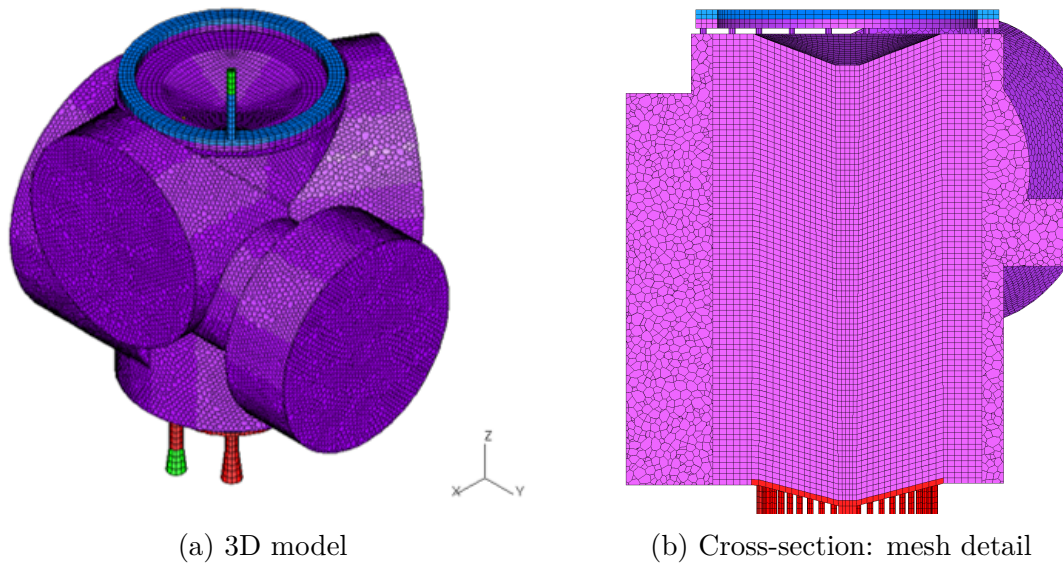


Figure 3.5: Combustion chamber model for 3D-CFD simulation

is shown in figure 3.5.

The chamber is kept at constant volume with a steady environment, where only the conditions of pressure are modified according to the values of chamber pressure defined at the test bench.

The initialization of the simulations include the definition of several input parameters, mostly already described when dealing with the definition of the injector geometry and the injection initialization. In the following the most important input parameters that were previously omitted are summarized:

- Cylinder initial temperature: initial temperature of cylinder environment, cylinder walls, head, liner and piston crown should be defined.
- Engine speed: engine speed is kept always constant at 1667 [*rpm*].
- Droplets per parcel (dpp): the number of dpp has influence on the accuracy of the simulation, and on the calculation time. Generally, once fixed a value of injected droplets during injection and a value of initial SMD, the number of dpp must be adapted.

One of the tasks carried out in this work is to define a methodology to chose the set of initialization parameters that allows to obtain the most accurate possible simulation's output. The parameters objects of variations are the one defining the injector geometry and the droplets initialization, since the experimental analysis provides data that could be used as a reference for the calibration of the injection

model. This procedure is the only one that allows improvements in the quality of the simulation. The next chapters will discuss in detail the most important steps in the development of this methodology, in terms of considered parameters, possible variations, influence on simulation results, and final choices.

The following table summarize the values adopted at the beginning of this analysis for the main simulation's parameters:

P_r	100 – 200 [bar]
P_k	1 – 5 – 10 [bar]
T_{fuel}	333 [K] → fuel properties chosen at this temperature
$T_{chamber}$	300 [K]
α, γ	9.5° → from spray targeting. The two angles have same value for multi-hole injectors
L_{min}	1 [mm]
L_{max}	8 [mm]
dpp	1000 [–]
SMD	10 [μm]
Engine speed	1667 [rpm]
v	speed calculated from Bernoulli equation depending on Δp

Table 3.1: First choice of simulation's parameters

The post-processing of the simulations is aimed to obtain results in terms of geometry, kinematic, and thermodynamic of the spray during its development, thus compare the output of the simulations with the results obtained from the experimental analysis, make statements about the quality and the accuracy of the injection simulation, and apply possible modifications to the injection model in order to obtain improvements. The comparison of the results is performed by means of a Matlab tool which derive from the one described in Chapter 2, used for the analysis of experimental videos. In this case, firstly frames showing the spray propagation, output of the simulation, are analysed, then the comparison is carried out between the two sets of data (experimental and simulation).

The 3D-CFD allows also to study in detail the characteristics of the single injected droplets, like the SMD distribution and the evaporation of the liquid fuel, during the injection. This additional study is essential in the understanding of the spray behavior under different injection conditions, and allows to make a critical comment about the veridicity of the simulation.

Chapter 4

3D-CFD Simulation of Injection - Calibration of Initialization Parameters

The first step in the attempt of improving the injection simulation model in *QuickSim* is the understanding of which are the most important parameters in the setup of the simulation, and what is their influence on the final results.

This chapter is dedicated to the study of the injection initialization parameters aimed to find a set of criteria to be used to define the values that provide the best possible quality of the simulation. A fundamental aid is given by the experimental data collected in the analysis of the test campaign, which can be exploited to calibrate the injection initialization parameters in a more precise and faster way. This procedure is essential in *QuickSim* since the droplets are initialized in a certain spacial domain in the proximity of the injector tip, and they are characterized by some quantities that should take into account the effects of internal nozzle flow and primary breakup, processes not investigated by the software.

As already mentioned before, the considered quantities are the ones related to the definition of the injected fuel droplets, and the most influential are: velocity, initialization domain, spray angles, and Sauter Mean Diameter (SMD).

After the simulations, a comparison with experimental results is performed, where particular focus lies on the analysis of axial penetration. In fact spray penetration is commonly used as comparative means for different reasons: firstly because of its practical importance (e.g. optimization of spray penetration in ICE), secondly because this parameter is easily measurable and can be used for models' validation, finally because a correct prediction of the spray penetration can indirectly indicate the correctness of complex models of spray formation [12].

In this calibration phase, the simulations are performed for the injector of type *F* under the following injection conditions, which will be referred to as standard

conditions:

- Injection pressure $P_r = 100$ [bar]
- Chamber counter pressure $P_k = 1$ [bar]
- Fuel density $\rho_{fuel} = 720.59$ [kg/m³]
- Mass flow rate $\dot{m} = 656.5$ [g/min]
- Injection duration $t_{inj} = 1.7$ [ms]

4.1 Fluid Exit Speed

The first analysed quantity is the velocity at which the fluid exits the injector. The default value is calculated from the Bernoulli equation 3.3, and it corresponds to the value of speed that the droplet of fluid would have in ideal conditions; the ideal value can be considered as the maximum value of speed that the fluid could reach as it is injected in the combustion chamber. Here the possibility of initializing the speed starting from the correspondent values obtained experimentally is investigated. Since the experimental speed is evaluated as $\frac{dx}{dt}$, the considered experimental speed is the one that is registered in the time interval in which the fluid travels from the beginning to the end of the initialization domain, which means when $L_{min} \geq x \geq L_{max}$.

Under standard conditions the values for ideal and experimental speed are:

v_{ideal}	165 [m/s]
v_{exp}	114 ÷ 108 [m/s]

The considered possible configurations for initialization speed are:

1. Constant value of speed: ideal speed
2. Constant value of speed: experimental speed
3. Speed profile: speed is initialized with a profile during the injection duration, and then is kept constant. The profile is a linear function between the two values of ideal and experimental speed. An example of the initialization speed profile under standard injection conditions can be found in figure 4.1.

Figure 4.2 shows the results obtained from the simulations listed above in terms of spray axial penetration. The curve obtained initializing the speed with a constant value equal to the experimentally obtained one shows a great difference with respect

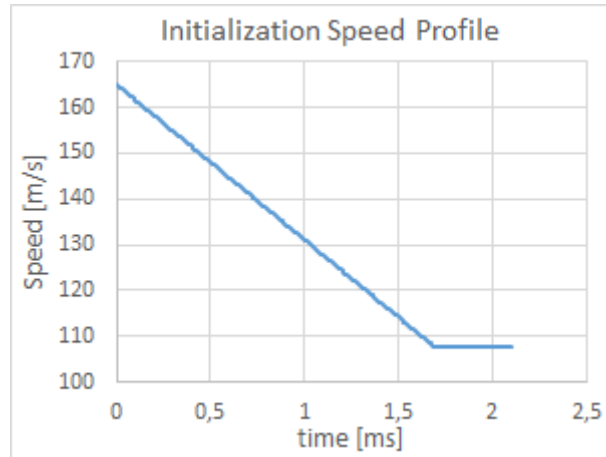


Figure 4.1: Initialization speed profile for standard injection conditions

to the experimental penetration curve, and only the final value seems reasonably comparable. On the other hand when the speed is initialized equal to the ideal speed, the curve does not present almost any deflection as expected after the first fast increase of penetration. The solution that consider both experimental and ideal speeds, with speed of initialization not constant, seems the most proper, as it provides a trend of the curve initially steep and a tendency to bend after a certain time.

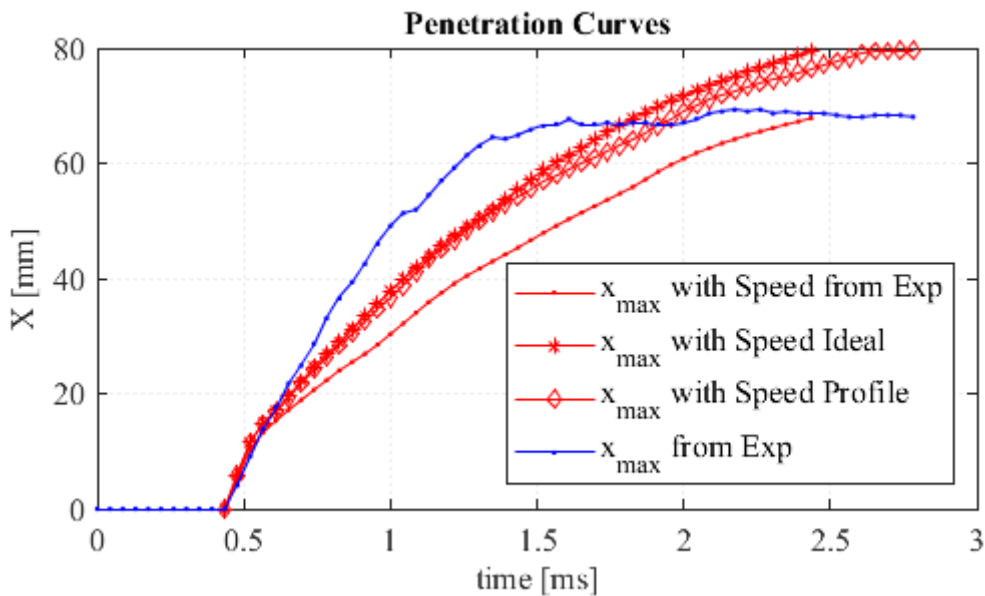


Figure 4.2: Speed calibration results

Considering the reported penetration curves, some numerical results can be reported to make some conclusions about the choice of initialization speed.

Case	$x_{endofinjection}$	$\Delta x_{endofinjection}$	Δx	$error$
Constant ideal speed	74.4	5.9	6.2	13.4%
Constant experimental speed	63.5	5	11	21%
Speed profile	72	3.5	6.5	13.8%

Table 4.1: Speed calibration - numerical results

The best choice for the initialization of fluid exit speed is the one in which the experimental measurement and the ideal value are combined, but still the result is not satisfactory. As a matter of fact the penetration curve differs too much from the experimental one in terms of numerical values and trend. The motivations can lie in between the fact that the missing deflection of the curve from simulation could be caused by some fluid behavior models in the simulations (e.g. evaporation, breakup models), and on the other hand the experimental curve could be affected by spray detection methods (e.g. very dispersed spray, imaging tool not able to detect very small droplets which do not reflect enough light).

Further improvements can be obtained by means of the calibration of the other droplets initialization parameters, analysed in the following.

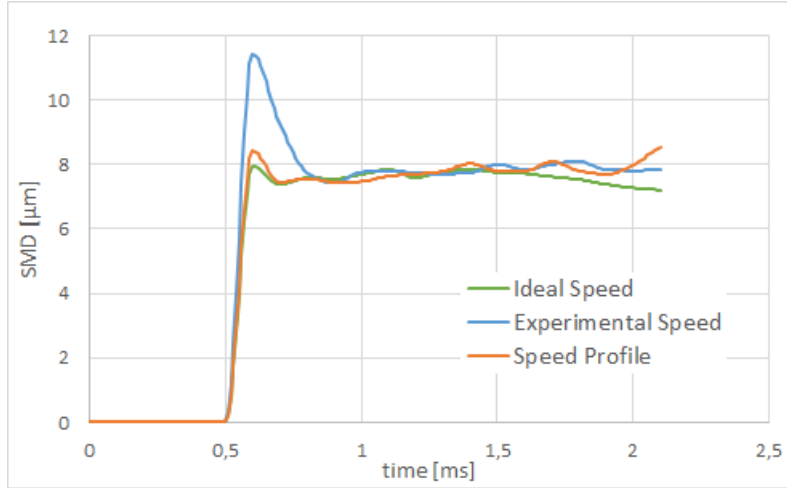


Figure 4.3: Influence of initialization speed on SMD distribution

The importance of initialization speed is reflected also in the droplets SMD distribution throughout the injection. Until now all the simulations have been performed considering a value for SMD of initialization of $SMD_{init} = 10 [\mu m]$, and the influence of initialization speed on the SMD distribution in a section of the spray

positioned at 30 [mm] from the injector tip is investigated. This influence can also dictate the final choice of initialization speed.

Figure 4.3 reports the obtained results. It is clear that an increase in the initialization speed leads to a reduction in the SMD of the droplets, especially in the initial part of the injection before reaching an almost constant value of droplets diameter. Anyhow the relation is not proportional and it is difficult to make predictions. Further simulations can prove the validity of this relation, as an increase of SMD of initialization limits the maximum achievable speed of the droplets.

4.2 Spray Angles and Initialization Domain

Spray angles that define the geometry of the jet (α and γ), and droplet initialization domain length (L_{min} and L_{max}) are expected to have an influence on the spray development and propagation.

The initialization domain has been implemented to better represent the position of the injector orifice with respect to the injector coordinate system position, and to consider the area of prevailing primary droplet breakup [5]. The definition of the two quantities L_{min} and L_{max} has influence on the spray penetration, on the spray pattern and on the fuel evaporation behavior, even if in a small amount. In this particular case these parameters are set equal to $L_{min} = 1$ [mm] and $L_{max} = 8$ [mm] respectively. Some simulations have been performed in order to evaluate the influence of modifications of both the lengths. In particular the attempts made investigate the results either with a lower value of L_{min} or an increase in L_{max} . An increase in L_{max} should theoretically cause an increase in spray penetration, but, in this specific application, the limited increase to $L_{max} = 9$ [mm] is not able to produce a significant effect, as shown in figure 4.4a. An analysis of the variation of L_{min} has shown similar results, and a combined increase of both the length, keeping the same ΔL corresponds only to a relocation of the injector coordinate system, with no effects on the spray development.

Concerning the angles describing the spray geometry, it is sufficient to focus on the angle α since the analysis is about multi-hole injectors. The value of the jet width angle adopted until now is the one provided by the injector manufacturer, which is $\alpha = 9.5^\circ$. The variation of the value of this angle is now investigated to find which is its influence on the fuel spray. In order to do so, simulations with lower value of α have been performed, and the results are reported in the following.

Figure 4.4b shows how a reduction in the value of angle α from 9.5° to 8.5° has the effect of increasing the penetration of the spray inside the chamber. This is mainly due to the fact that a smaller angle makes the jet thinner and faster in its central part, thus causing a consequent faster and deeper penetration of the spray.

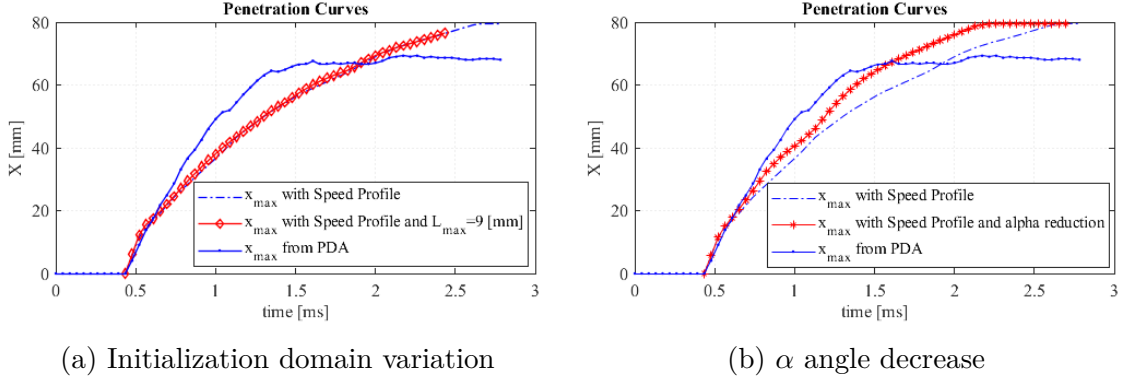


Figure 4.4: Initialization parameters variation

4.3 SMD of Initialization

Another fundamental parameter in the definition of the injected fluid characteristics is the diameter of the droplets, expressed in terms of SMD. The effects of the SMD on the spray formation are largely described in literature, and here it is considered the aspect relevant to this work, the effect of SMD of initialization of the droplets on the spray development. It is clear that as the diameter of the injected droplets increases, also the axial penetration of the spray tends to increase, due to the fact that a higher diameter corresponds to larger and more massive droplets, whose vaporization process is slower, thus allowing them to penetrate more inside the chamber.

The prediction and estimation of the correct values of SMD has been and is a crucial point in the injection simulation modelling. Several models and equations have been developed for this purpose, especially for more studied types of injector such as the hollow-cone injector, whose SMD can be calculated with equations like the one reported in the following [11]:

$$SMD = 4.52 \left(\frac{\sigma^{0.5} \mu^2}{\rho_a \Delta p^2} \right)^{0.25} h_s^{0.25} + 0.39 \left(\frac{\sigma \rho}{\rho_a \Delta p} \right)^{0.25} h_s^{0.75} \quad (4.1)$$

in which h_s is the thickness of the conical liquid sheet for hollow-cone injectors. The most suitable choice of the SMD of initialization is now investigated, with the goal of obtaining precise simulation's results and a desired SMD distribution in the spray. Different options are searched which comprehend cases with either constant or variable SMD of initialization in time. The reason why also a variable SMD of initialization is considered lies in the characteristics of the software *QuickSim*. Since the injector fluidodynamics and the primary breakup phenomena are not taken into account in the simulation, it is necessary to predict the outcome of the non-simulated phenomena by means of the initialization parameters.

After the calibration of the exit fluid speed, the necessary actions are aimed to increase the axial penetration in the first phase of injection, and enhance the subsequent deflection of the penetration curve. In order to do so the value of SMD of initialization is firstly increased from $SMD_{init} = 10 [\mu m]$ to $SMD_{init} = 15 [\mu m]$, keeping its value constant throughout the whole injection event. The results in terms of spray penetration are show in figure 4.5.

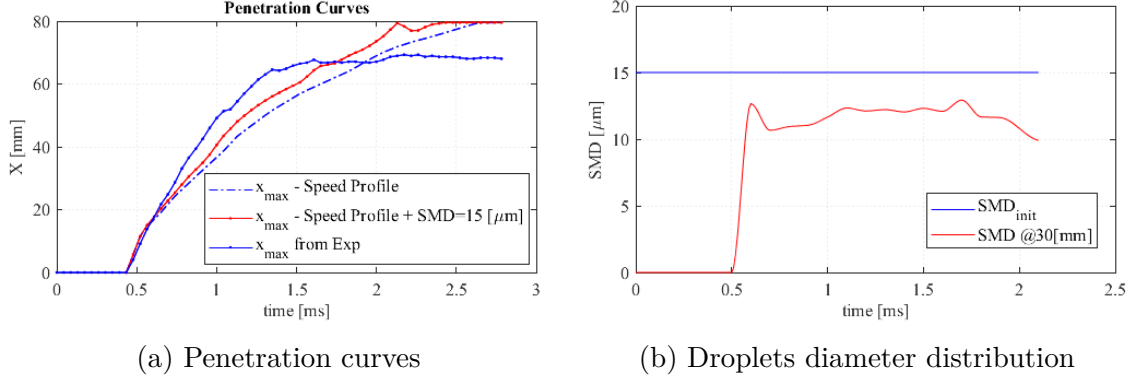


Figure 4.5: Results for simulation with higher SMD_{init}

This plot confirm the expected behavior of the spray in case of increased SMD of the injected droplets, and, for what concerns the obtained droplets diameter distribution, it has been observed the presence of a correlation between the constant value of initialization SMD and the values of droplets diameter obtained in a cross section of the spray at 30 [mm] from the injector tip. After an initial peak, the droplets' size stabilizes around a value which is approximately the 80% of the initialization value. This relation is exploited in finding more precise results by means of further simulations, which are characterized by variable SMD of initialization during the injection, in order to obtain better results and a desired trend of the droplets diameter curve. The simulations have been initialized with the following SMD conditions:

1.

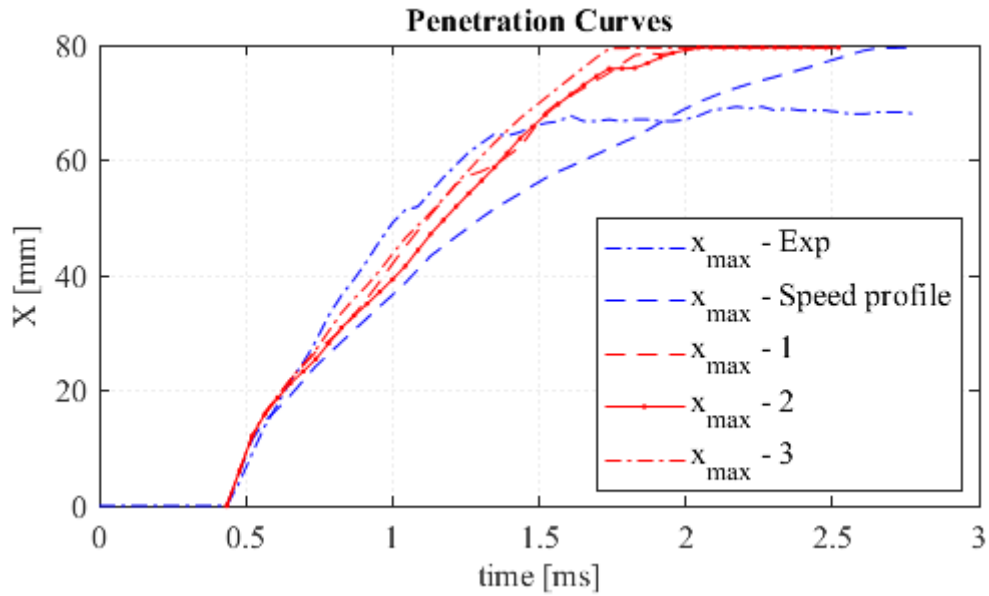
$$SMD_{init} = \begin{cases} 25 \div 9 [\mu m] & t \leq 1 [ms] ASOI \\ 9 [\mu m] & t > 1 [ms] ASOI \end{cases}$$

2.

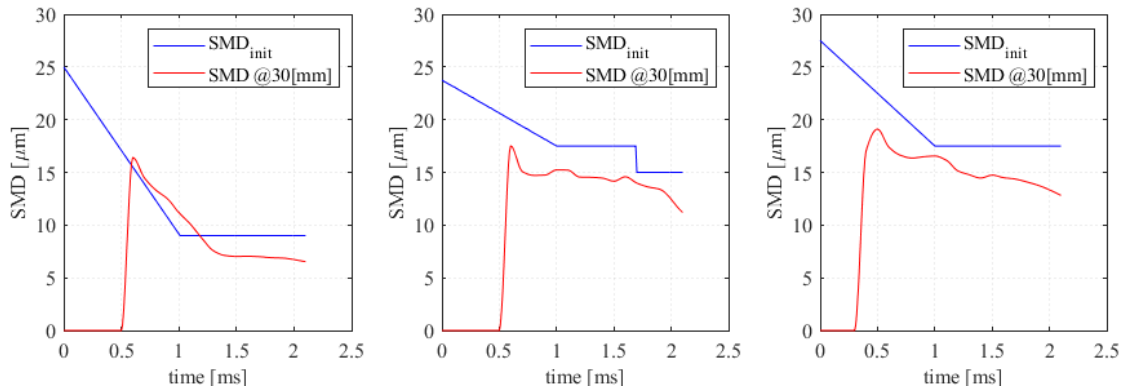
$$SMD_{init} = \begin{cases} 24 \div 17.5 [\mu m] & t \leq 1 [ms] ASOI \\ 17.5 [\mu m] & 1 < t \leq 1.7 [ms] ASOI \\ 15 [\mu m] & t > 1.7 [ms] ASOI \end{cases}$$

3.

$$SMD_{init} = \begin{cases} 27.5 \div 17.5 [\mu m] & t \leq 1 [ms] ASOI \\ 17.5 [\mu m] & t > 1 [ms] ASOI \end{cases}$$



(a) Penetration curves



(b) Droplets diameter distribution (options 1 - 2 - 3)

Figure 4.6: Results for variable SMD of initialization

Observing figure 4.6a it is possible to state that the adoption of a variable SMD of initialization, which follow a ramp function for a certain time, and then it is kept constant, helps in obtaining a distribution of the droplets diameter which follows a typical curve with an initial peak, due to the fact that the first droplets which reaches the studied spray cross section are the biggest, heaviest and fastest, and then it stabilizes around an almost constant value. The final choice between the suggested options will be the one which offer the most accurate results in terms of reproduction of spray development and propagation, in this case the option number 3.

4.4 Final Choices and Results

After having understood which are the effects of the single investigated parameters, the final step is finding a set of criteria in the choice of how each parameter should be initialized before a simulation aiming to the best possible combined effect. Among the analysed quantities, the most influential ones are the fluid exit speed, the angle α and the Sauter Mean Diameter. The initialization domain definition has no tangible effect if not modified significantly. Anyhow, in order to facilitate the process, the only considered parameters in this procedure will be the fuel exit speed and the SMD. The angle α can be maintained at the value provided by the injector manufacturer, with an imposed peak in the initial instants of the injection used to reproduce the peak observed in the experimental tests analysis.

Best solution for the initialization of the fuel speed is to consider both the ideal value calculated with Bernoulli equation, and the values obtained experimentally. The suggestion made here is to interpolate the speed between these two values throughout the whole duration of the injection.

The initialization of the SMD is more complex and requires an estimation also based on the level of underestimation of the spray penetration expected by the CFD software. The characteristics of the *QuickSim* tool push towards the adoption of a variable SMD of initialization, in order to best reproduce the correct droplets SMD distribution and to obtain coherent and reliable results.

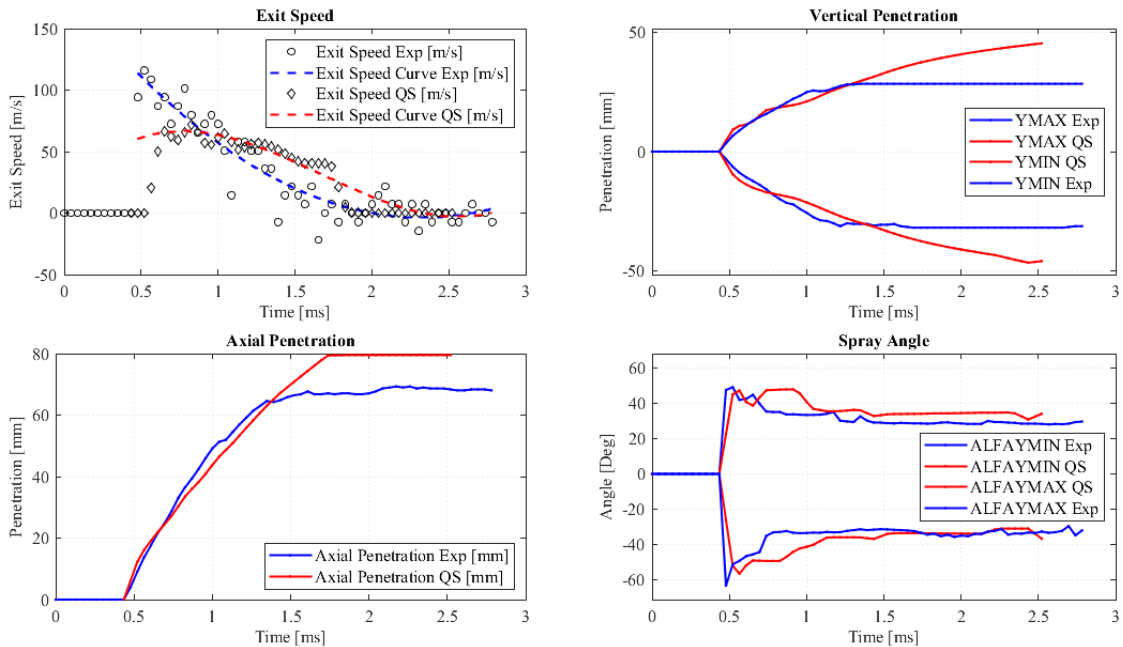


Figure 4.7: Calibration of initialization parameters - Final results

Figure 4.7 shows the final results obtained with the selected best set of initialization parameters, which are listed in the following:

Parameter	Chosen value
Angle α	9.5° and 30° in the first 0.3 [ms] of injection
Initialization domain	$L_{min} = 1$ [mm], $L_{max} = 8$ [mm]
Fuel exit speed v	Speed profile from ideal to experimental over injection duration ($165 \div 108$ [m/s])
<i>SMD</i>	Ramp for 1 [ms], then constant (see option 3 on page 47)

Table 4.2: Calibration of initialization parameters - Final choice

The simulation provides a good level of reproduction in all the investigated quantities. The vertical penetration comparison is limited due to the edges of the frames in experimental analysis, but the good approximation of spray angle and axial penetration give sufficient proofs to state that the simulation's quality is satisfactory. The axial penetration is very precise in the first part of the injection event, where the spray propagates very fast inside the chamber. The following divergence of the curves is due to the uncapability of the imaging software to recognize very small droplets, and possible other reasons related to the fluid behavior models in the simulation. However in analysis of spray penetration, the importance is the progression of penetration length in a short time, since the fast spray formation is more crucial rather than fully developed spray length to achieve better combustion [19]. Nevertheless, the overall error between experimental results and simulation is now around 10%, making the simulation very accurate.

Figure 4.8 shows the comparison between the analysis of experimental tests and calibrated simulation in the standard case of injection pressure $P_r = 100$ [bar] and chamber pressure $P_k = 1$ [bar].

The next phase is dedicated to the analysis of injection events under different injection conditions in terms of injection pressure and chamber counter pressure. This analysis is able to provide information about the sensibility of the 3D-CFD software to the injection conditions, on the basis of which some considerations can be made on how the injection model should be modified and adjusted according to them.

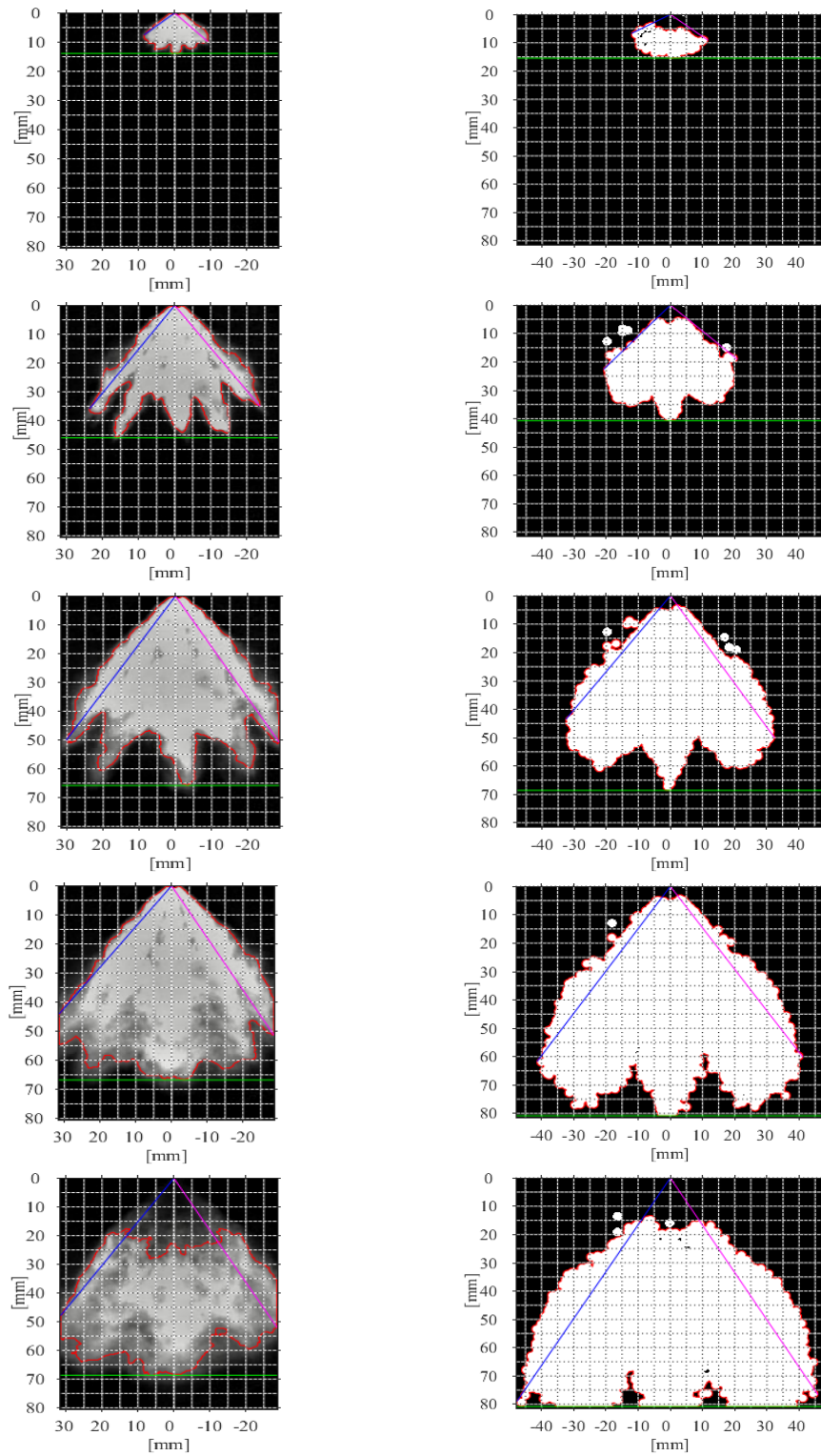


Figure 4.8: Analysed frames: Experiments (left) and Simulation (right)

Chapter 5

3D-CFD Simulation - Variation of Injection Conditions

After having obtained satisfying results in terms of quality of the injection simulations under standard injection conditions ($P_r = 100$ [bar], $P_k = 1$ [bar]), the expectation is to observe a good approximation of the injection experimental tests also for injection simulations performed under different conditions. This chapter is dedicated to the analysis of the results obtained for simulations under different injection conditions, aimed to validate the methodology developed for the injection model in *QuickSim*. In the cases in which unsatisfactory results are observed, an investigation about possible encountered problems and applicable solutions is performed in order to complete the process of improvement of the injection simulation. In general it must be taken into account the fact that a variation in the injection conditions should be accompanied by adjustments of the other quantities involved in the spray definition, such as the delta pressure over the injector nozzle, the fuel exit speed, the thermodynamic properties of the air inside the chamber. In the performed simulations the temperature of the injected fuel and the temperature of the chamber ambient gas (constant volume chamber in which the pressure is controlled) are not modified.

The possible configurations for the analysed injection events derive from the combination of these parameters:

- Injection pressure $\rightarrow P_r = 100, 200$ [bar]
- Chamber counter pressure $\rightarrow P_k = 1, 5, 10$ [bar]

In the following the results of different simulations are reported shortly, keeping the focus on how the variation in injection and chamber pressure influence the solution of the simulations.

5.1 Simulations Results with Variation of Injection Conditions

Injection conditions have influence on the spray development and propagation both from a kinematic and thermodynamic points of view. Chapter 2 has provided a description of the observed behavior at the test bench. The configurations adopted for experimental tests have been reproduced in the simulation environment, and here the results are reported with respect to the experimental data.

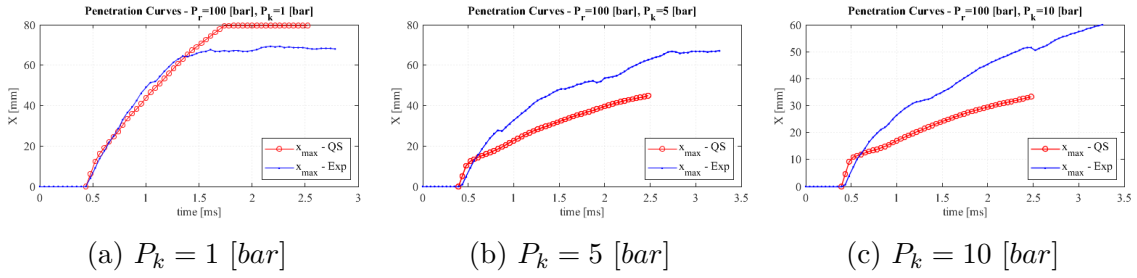


Figure 5.1: Penetration curves - $P_r = 100$ [bar]

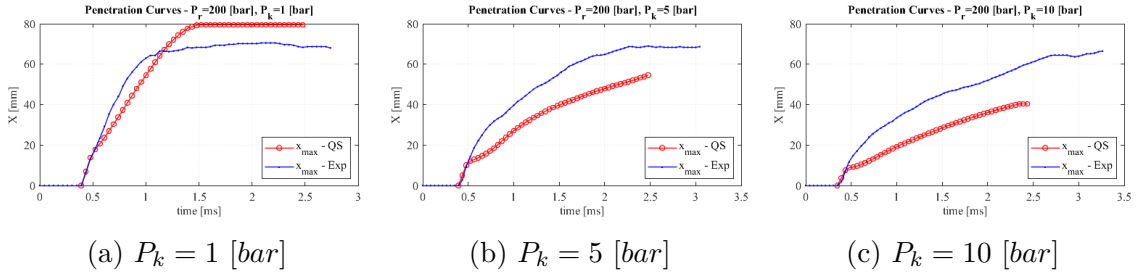


Figure 5.2: Penetration curves - $P_r = 200$ [bar]

The set of plots shown in figure 5.2 can be used as reference for the following observations about the effects of injection conditions on the results, in terms of kinematic of the spray, of the injection simulations.

An increase in injection pressure, at equal level of chamber counter pressure, causes, as expected, an increase in the axial spray penetration, due to a larger ΔP across the injector nozzle which result in an higher velocity of the injected fuel. The higher momentum of the droplets favours a faster penetration and a slower evaporation rate of the droplets. The quality of the simulation's approximation is not majorly affected in the case with chamber counter pressure of $P_k = 1$ [bar], with an error over the injection period of 14%.

The variation of chamber counter pressure has a great impact on simulation results.

Figures 5.1b, 5.1c, 5.2b, 5.2c are the considered cases. Theoretically an increase in chamber counter pressure corresponds to a reduction in the ΔP across the injector nozzle, a reduction in the injected fuel velocity and an increase in air density (from $\rho_{air} = 1.177 [kg/m^3]$ to $\rho_{air} = 5.806 [kg/m^3]$, and $\rho_{air} = 11.612 [kg/m^3]$). These conditions create a chamber environment more difficult to penetrate for the injected droplets, thus obtaining a slower and less deep spray axial penetration. This is confirmed by other studies like in [13], and by the presented experimental tests and simulations, although in this study the difference between experimental and simulation results is very large, and clearly not acceptable (error also greater than 20%). The reasons related to this error can be tracked down to the characteristics of the software, which provide a chamber environment very aggressive, and a big underestimation of the spray penetration. The problems seem to be related only to the propagation of the spray, in fact the distribution of the spray angle is well fitted by the simulations, suggesting that the overall shape of the spray is correctly reproduced, see figure 5.3.

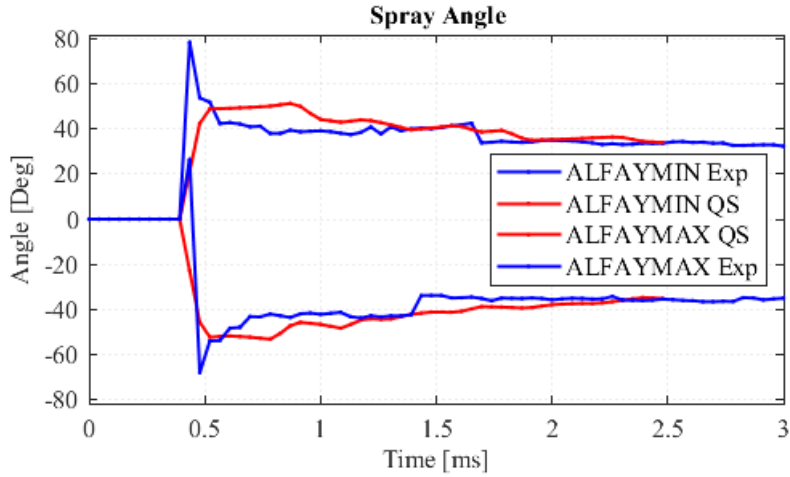


Figure 5.3: Spray angle for $P_r = 100 [bar]$, $P_k = 10 [bar]$

Further information are provided by the analysis of velocity and turbulent kinetic energy inside the chamber for different values of chamber pressure in figures 5.4 and 5.5.

From the critical observation of these results it is possible to identify the main problems related to the performed simulations. The simulation injection model seems more sensitive to variations in the thermodynamic state of the chamber environment than the real case, resulting in a premature decay of droplets speed and spray propagation.

In order to improve the quality of the simulation under every injection conditions

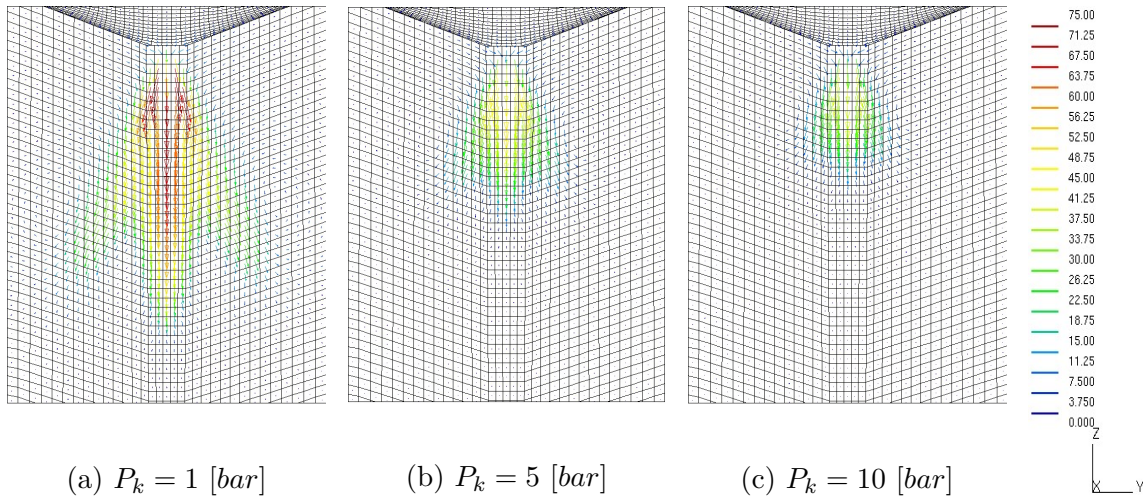


Figure 5.4: Speed vectors inside the chamber [m/s] - $P_r = 100$ [bar]

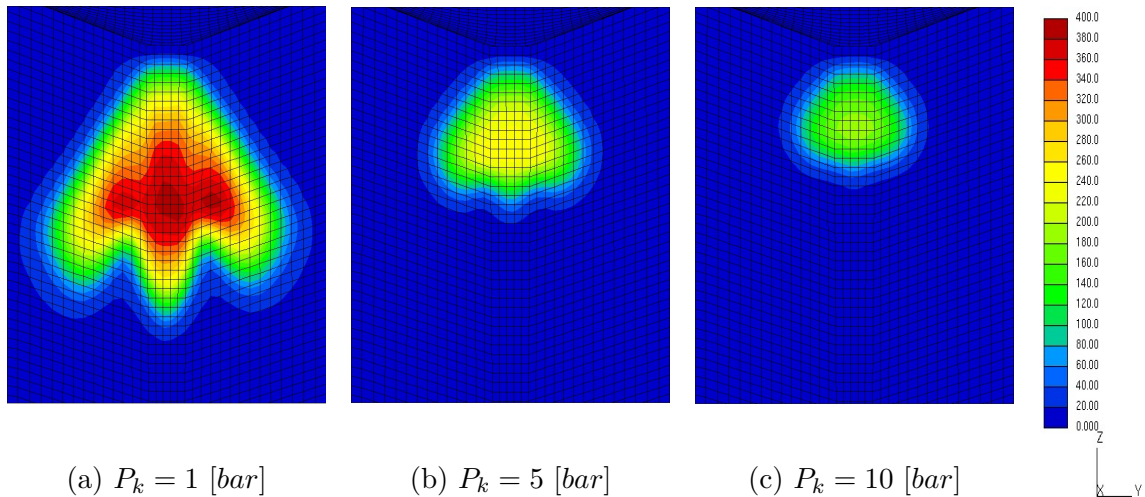


Figure 5.5: Turbulent Kinetic Energy inside the chamber [m^2/s^2] - $P_r = 100$ [bar]

it is necessary to somehow adapt the injection model to the injection pressure and chamber counter pressure, compensating their excessive effects on the spray propagation. Different solutions are explored in the following sections, and are here summarized:

- Investigation of the software's models for the description of the fluid behavior, such as liquid droplets breakup, evaporation, turbulence, etc., with particular focus on the breakup models, which are the easiest models to manipulate in the simulation initialization phase.
- Insight into the properties of ambient fluid (air), and how they are modeled

in the simulation environment (density, viscosity, specific heat, conductivity, turbulence).

- Possibility of strong modification of the initialization droplets SMD, in order to compensate the premature drop in the droplets kinematic properties. This solution could provide very precise geometry and kinematic reproduction of the spray, but may have non representative results in terms of fuel vaporized mass, thus influencing further analysis about mixture formation.

5.2 Fluids Behaviour Models

This section is dedicated to a deeper insight into the different models implemented by the 3D-CFD software which describe the behavior of injected fluid and ambient fluid, and their interactions. In particular the different droplets breakup models are studied in detail in order to reach a consistent level of understanding of how they work and how they can be exploited to obtain more accurate results.

5.2.1 Breakup Models in *QuickSim*

The *QuickSim* tool exploits the models incorporated in the software Star-CD for breakup of liquid droplets in a gaseous stream. As already mentioned, the peculiarity of the *QuickSim* tool is that it consider only the secondary breakup of the liquid droplets, since primary breakup and internal nozzle flow are taken into account by the definition of the initialization domain. The available secondary breakup models are:

- Reitz and Diwakar model
- Pilch and Erdman model
- Hsiang and Faeth model
- KHRT model
- User defined models

Each model provides a criterion for the onset of breakup, and for the estimation of the droplets diameter and the characteristic time scale of the breakup process.

The default setting in *QuickSim* operations is the Reitz and Diwakar model, but the following analysis is aimed to select the most suitable model for the description of the investigated high-pressure fuel sprays, providing satisfactory results under a variety of injection conditions.

Reitz and Diwakar

According to this model, droplet breakup occurs due to aerodynamic forces acting at the interface between liquid droplets and surrounding air. The action of these forces can be modeled as wave perturbations on the droplets' surface characterized by a certain growth rate and wavelength. The instability generated by these perturbations causes the droplet breakup, thus reducing the droplet's diameter. The rate of the diameter reduction depends on the combination of surface tension and inertia forces [13].

In the software application, this model considers two possible breakup regimes [8]:

- *Bag breakup*: non-uniform pressure field around the droplet causes it to expand in the low-pressure wake region and eventually disintegrate when surface tension forces are overcome.
- *Stripping breakup*: process in which liquid is sheared or stripped from the droplet surface.

The criteria for the onset of breakup are reported in detail in chapter 3, and here summarized:

$$\begin{cases} We = \frac{\rho|u-u_d|^2 d_D}{2\sigma_D} \geq C_{b1} \\ \frac{We}{\sqrt{Re_D}} \geq C_{s1} \end{cases} \quad (5.1)$$

And the correspondent characteristic breakup times are:

$$\begin{cases} \tau_b = \frac{C_{b2}\rho_d^{1/2}d_D^{3/2}}{4\sigma_D^{1/2}} \\ \tau_s = \frac{C_{s2}}{2} \frac{\rho_D^2}{\rho} \frac{d_D}{|u-u_D|} \end{cases} \quad (5.2)$$

The droplet diameter after breakup is estimated by means of the equation:

$$\frac{dd_D}{dt} = -\frac{d_D - d_{D,stable}}{\tau} \quad (5.3)$$

where $d_{D,stable}$ is the stable droplet size, which is the value of droplet diameter which satisfy the equalities of equation 5.2.

The adjustable constants C_{b1} , C_{b2} , C_{s1} , C_{s2} can be modified, within certain limits, in order to enhance or damp the growth of instabilities which lead to the breakup of the droplets. The breakup model is less aggressive when these modifications are applied to the mentioned parameters: C_{b1} and C_{b2} are increased, C_{s1} and C_{s2} are decreased. This condition is also the one responsible for highest values of observed spray axial penetration, since it provides higher values for critical Weber number.

Pilch and Erdman

According to the correlations developed by Pilch and Erdman, the breakup occurs if the droplet's Weber number is greater than a critical value

$$We_c = 12(1 + 1.077(Oh)^{1.6}) \rightarrow We_d > We_c \quad (5.4)$$

This model consider five different breakup regimes, defined by intervals of Weber number value, which are characterized by a specific dimensionless total breakup time T . The total breakup time τ and the droplet stable diameter are function of the breakup regime:

$$\tau = T \frac{d_D}{|u - u_D|} \left(\frac{\rho_D}{\rho} \right)^{1/2} \quad (5.5)$$

$$D_s = We_c \frac{\sigma_D}{\rho |u - u_D|^2} \left(1 - \frac{V_D}{|u - u_D|} \right)^{-2} \quad (5.6)$$

where $V_d = |u - u_D| \left(\frac{\rho}{\rho_D} \right)^{1/2} (0.375T + 0.0074T^2)$.

Hsiang and Faeth

This model is valid for value of Weber number $We < 1000$ and covers all types of breakup that are of interest in Diesel engine spray applications.

The breakup occurs if the following relation is satisfied:

$$We = \frac{\rho |u - u_D|^2 d_D}{2\sigma_D} > 6 \quad (5.7)$$

And the characteristic breakup time is:

$$\tau = \frac{5}{1 - (Oh/7)} \frac{d_D}{|u - u_D|} \sqrt{\frac{\rho_D}{\rho}} \quad (5.8)$$

The value of the Weber number which has to be overcome for the onset of the breakup can be modified in Star-CD by the user.

Kelvin-Helmholtz/Rayleigh-Taylor (KHRT)

The KHRT model for droplet breakup is an hybrid model that combines the Kelvin-Helmholtz wave model for aerodynamic instabilities growing on a droplet surface with a model that considers Rayleigh-Taylor instabilities resulting from the deceleration of the injected droplets.

The combination of these two models with the concept of breakup length has allowed to obtain compliance between predicted spray behavior and experimentally observed trends in past studies [14]. The liquid breakup length depends strongly on nozzle geometry effects and the injection velocity.

The injected droplets are subjected to the Kelvin-Helmholtz model until they reach the breakup length, after which also the Rayleigh-Taylor criteria are introduced. After the droplets pass the breakup length the two breakup models compete with each other and the one predicting the fastest onset of an instability gives rise to a breakup event.

The two competing models are characterized by different droplets breakup processes, schematically shown in figure 5.6:

- KH wave model: in a breakup triggered by the KH process a parent parcel with radius larger than the wavelength Λ_{KH} of the growing unstable surface wave breaks up to form a new parent and child droplet pair. The size of the stable child droplet is:

$$D_{s,KH} = 2B_0\Lambda_{KH} \quad (5.9)$$

where Λ_{KH} is the wavelength corresponding to the disturbance wave with maximum growth rate Ω_{KH} , and B_0 is a model constant, usually set equal to 0.61.

The characteristic breakup timescale is calculated as:

$$\tau_{KH} = \frac{3.726B_1D/2}{\Lambda_{KH}\Omega_{KH}} \quad (5.10)$$

where B_1 is another model constant with default value of 40, but it can vary in the range between 10 and 60 [14].

- RT model: the RT model predicts instabilities on the surface of the drop the grow for a time greater than the characteristic timescale, after which the droplet finally breaks up into new droplets of different sizes, whose number is adjusted to conserve the mass and number of original parcels. The condition for the breakup to occur is related to the diameter of the droplet:

$$D > C_3\Lambda_{RT} \quad (5.11)$$

where C_3 is a scaling constant with default value of 0.1.

The characteristic breakup timescale is calculated as:

$$\tau_{RT} = \frac{C_\tau}{\omega_{RT}} \quad (5.12)$$

where C_τ is a model constant usually set equal to 1, $\omega_{RT} = \omega(k_{RT})$ is the maximum growth rate of the surface disturbance, and $k_{RT} = 2\pi/\Lambda_{RT}$ is the wavenumber that maximizes the growth rate.

The KHRT model is characterized by the presence of four adjustable parameters B_0 , B_1 , C_3 , C_τ , two for KH model and two for RT model, that can be modified in the settings of the simulation, thus allowing to set the values for these constants which provide the best reproduction of experimental results.

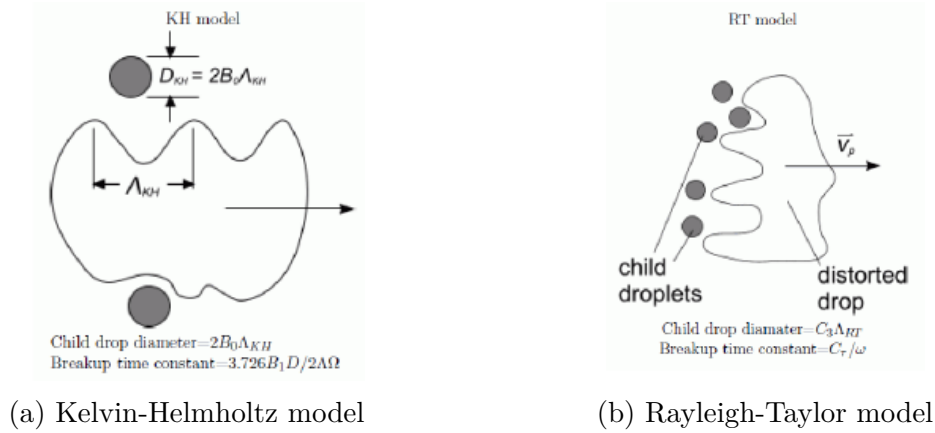


Figure 5.6: Differences in the KH and RT breakup models

5.2.2 Description of the Environment Fluid

A further option in the process of improving the injection simulation is to understand how the software describes the properties of the fluid inside the chamber, in which the liquid fuel is injected. In this application the chamber contains air.

The software allows the user to select how the thermodynamic properties of the fluid are defined and the applied turbulence models. The considered properties are the density, the molecular viscosity, the specific heat and the conductivity. Each of these quantities can be modeled by user functions, ideal laws, constants, or by other equations.

An analysis has been performed to understand which are the effects of the application of different models for these properties on the final simulation results. The final goal of this analysis is to investigate possible cause of the particularly high sensitivity of the injection simulations to variations in the chamber pressure.

However the obtained results have not shown significant differences with respect to the case with default settings. For example, the density of the gas, previously defined by a user function of temperature and pressure, have been defined by means of the ideal gas law, and different real gas laws, but the simulations have not provided results with differences worth of further investigation.

The turbulence models have not been investigated, since a detailed analysis of the turbulence effects on the injection would have required a consistent time effort. The selected turbulence model is the k - ϵ model for high Reynolds number, and it has not been modified.

5.3 Application of Different Breakup Models

Among the different breakup models implemented in Star-CD and accessible by *QuickSim* the Reitz and Diwakar model and the KHRT model have been selected as the most suitable for this analysis. The reasons of this choice lie in the fact that these two models are the ones that can be modified easily according to the application, thanks to their adjustable parameters in the definition of the breakup onset condition and the characteristic breakup timescale.

Here the goal is to investigate the application of different breakup models, properly initialized, in order to improve the quality of the simulations, and overcome the divergence between simulation and experimental results shown in the previous section. The starting point is again the simulation under standard injection conditions for the understanding of how to treat the models' constants, and then the analysis will be focused on the definition of the best breakup model and the way to proceed in the set up of simulations under different injection conditions.

In order to apply a correct modification of the adjustable parameters, it is necessary to understand their meaning.

In Reitz and Diwakar model there are two critical values after which instabilities arise, and two parameters which modify the breakup timescales and they are basically a measure of the evaporation rate of the droplets.

In KHRT model two parameters regulate the KH wave model, and other two parameters regulate the RT model. Within each of these pairs one parameter scales the radius of the new children droplets (B_0 , C_3), and the other acts on the breakup time (B_1 , C_τ).

5.3.1 Standard Injection Conditions

Firstly the application of different breakup models to simulations under standard injection conditions ($P_r = 100$ [bar] and $P_k = 1$ [bar]) is performed.

In this case the goal is to make the breakup model more aggressive in order to reproduce the deflection in the penetration curve encountered analysing experimental data, and until now not present in simulation results. In order to do so two attempts have been made:

- Reitz and Diwakar model $\rightarrow C_{b1} = 3.6$ (\downarrow), $C_{b2} = 2$ (\downarrow), $C_{s1} = 0.5$, $C_{s2} = 20$
- KHRT model $\rightarrow B_0 = 0.61$, $B_1 = 40$, $C_3 = 0.1$, $C_\tau = 9$ (values selected from literature [14])

Figure 5.7 reports the results in terms of spray axial penetration.

These plots suggest that the best fitting of the experimental penetration curve is obtained adopting the KHRT breakup model, which provide a deflection of the

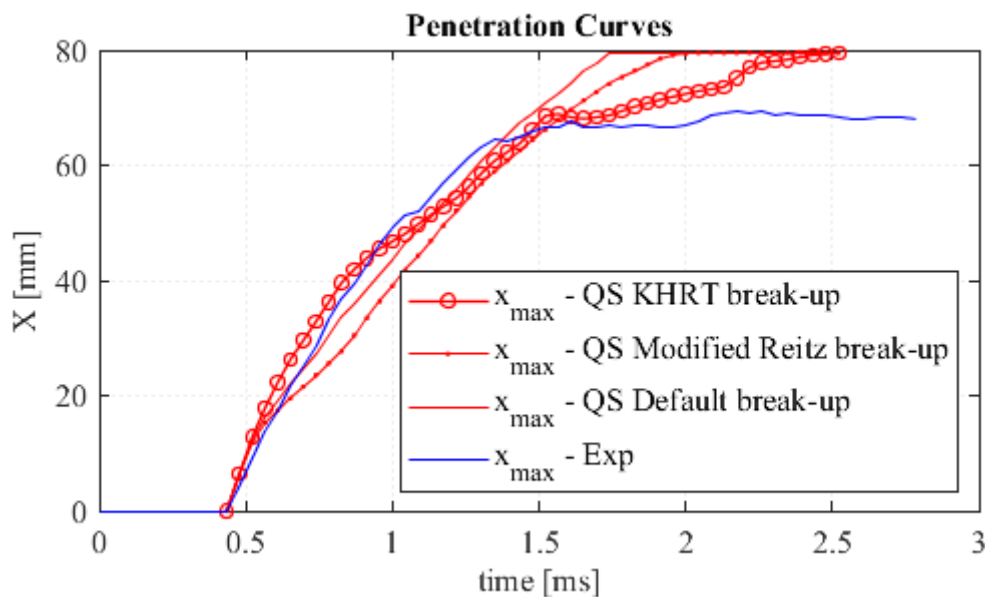


Figure 5.7: Penetration curves from simulations with different droplets breakup models

curve, as necessary, and closer punctual values, with a reduction in the mean error from 12% to approximately 9%. Also the other quantities (spray angle, exit fuel speed, vertical penetration) are well approximated, as can be seen in figure 5.8.

The application of the KHRT breakup model has influence also on the droplets diameter distribution registered at a spray cross section at 30 [mm] from the injector tip. As shown in figure 5.9, the adoption of the KHRT model enhances the presence of the initial peak in the SMD curve, as expected by this type of curve, and since the breakup model has been modified to be more aggressive the higher level of instabilities on the droplets and higher evaporation rate make the value of droplets diameter lower with respect of the previous case, as expected.

5.3.2 Variation in Injection Conditions

Simulations with increased values of injection pressure and chamber counter pressure, with respect to the standard case, have shown how the simulation environment suffers of high sensitivity to these variations, resulting in a significant underestimation of the spray penetration in the chamber. Therefore the decision of intervene on the breakup models. The application of less aggressive breakup models should be aimed to compensate the resistance that the ambient fluid exerts against the injected liquid fuel. Several simulations have been carried out to find the right way to adapt the models to each injection condition.

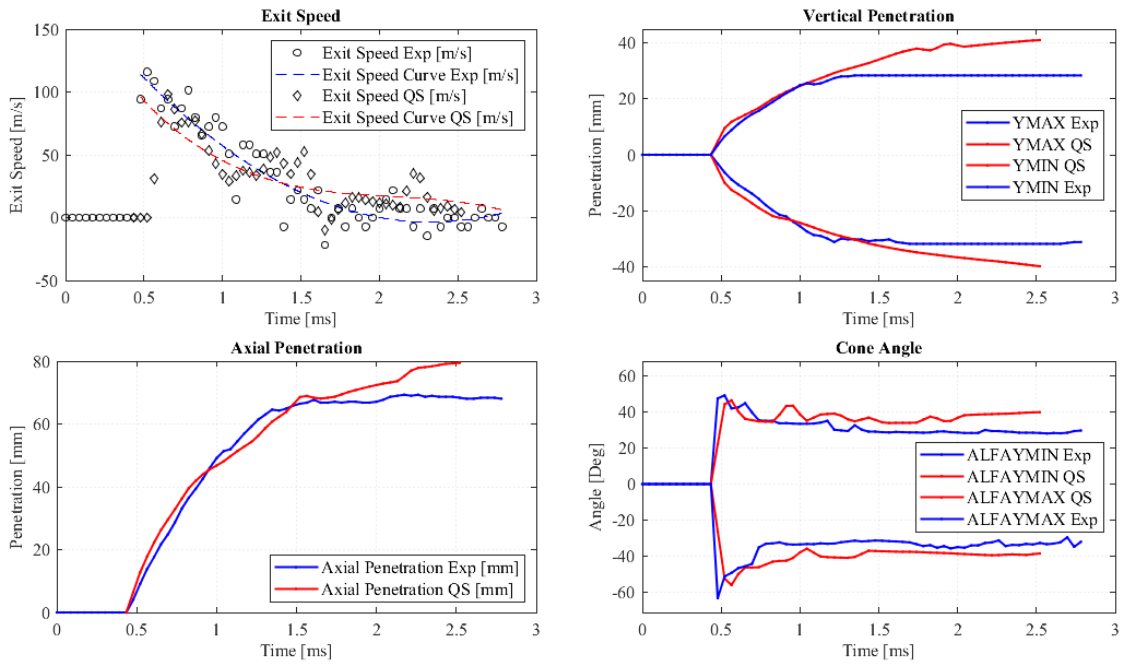


Figure 5.8: Results for simulation in standard injection conditions with KHRT breakup model

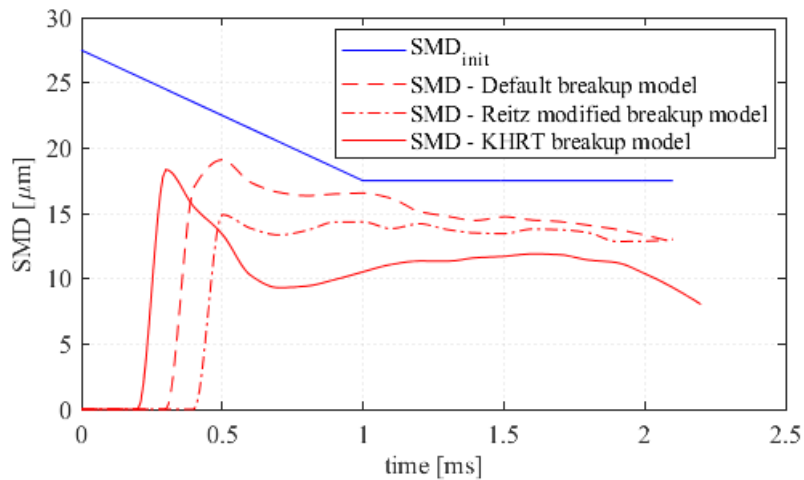


Figure 5.9: Droplets diameter distribution at 30 [mm] from injector tip - Standard injection conditions and different breakup models

The applied modifications to the breakup models by means of their adjustable parameters are basically the reduction of the evaporation rate, the increase of critical values for the onset of instabilities, the increase of the value of children droplets'

diameter.

Reitz and Diwakar and KHRT were the models adopted. Several configurations of their parameters have been attempted with decreasing levels of aggressiveness of the breakup. In the following only the most important results are reported, which have been obtained with the KHRT breakup model in which the main modifications involve the constants B_1 and C_τ regulating the breakup timescale of the two submodels, thus the evaporation rate. Figure 5.10 reports the penetration curves resulting from simulations under different injection conditions, highlighting the difference between the used breakup models.

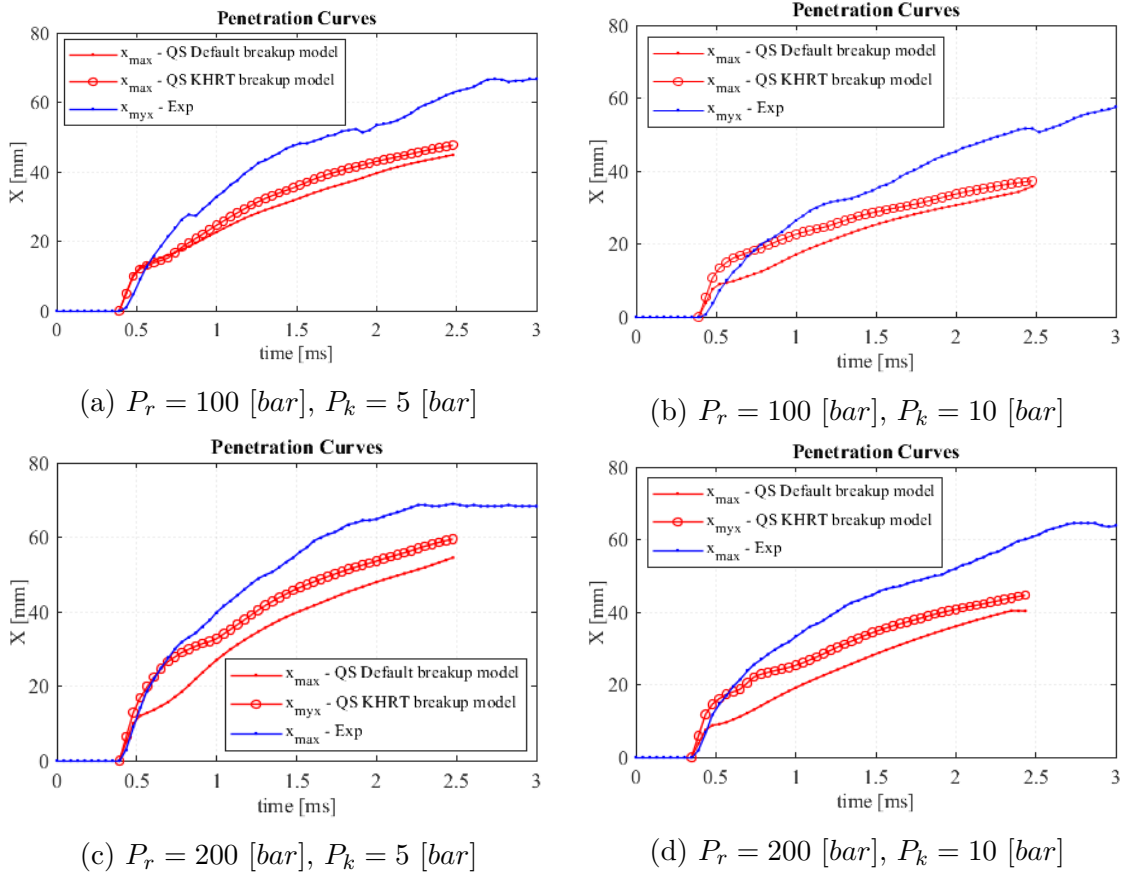


Figure 5.10: Effects of breakup models in a variety of injection conditions

The applied modifications provide improvements in the results, but still the experimental curves are well fitted only in the early phase of the injection. The criticalities related to the increase in chamber counter pressure are less important, especially in the cases with increased injection pressure, but still present. The mean error between the experimental and simulation curves is still greater than 15% in the best

case. The error increases as the chamber pressure increases, but the effects are not proportional.

In addition to this it must be kept into account that modifications of the breakup models aimed to get them less or more aggressive have consequences on the vaporization of the injected fuel. Figure 5.11 reports an example of this fact in the case of $P_r = 100$ [bar] and $P_k = 5$ [bar], where the breakup model is made less aggressive.

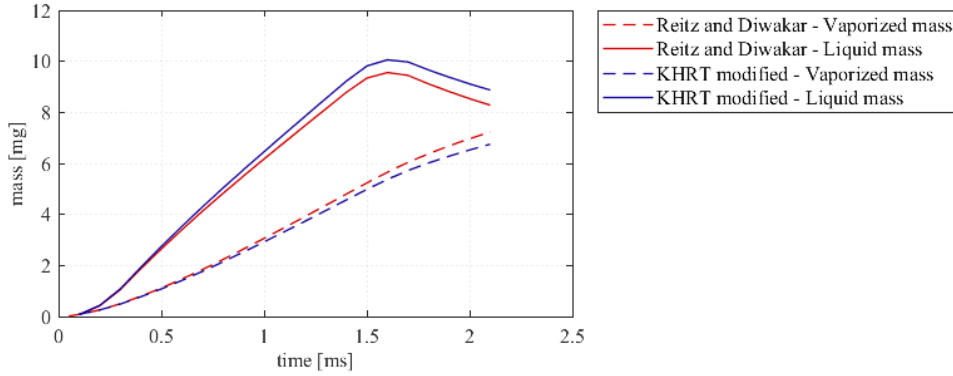
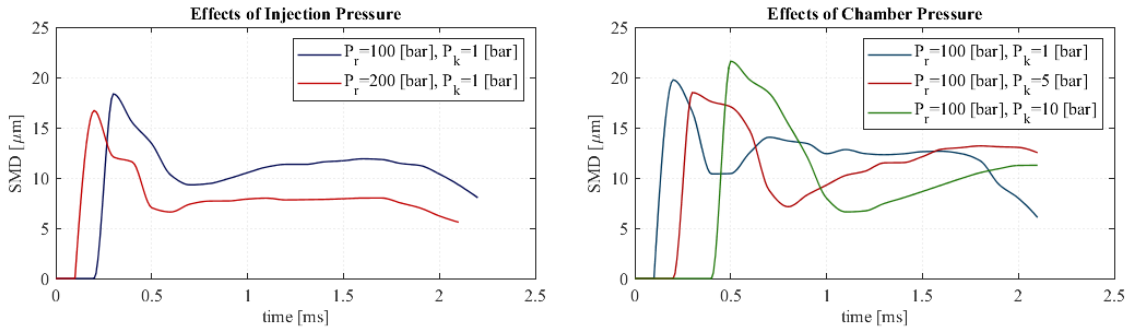


Figure 5.11: Effect of breakup model modification on the fuel vaporized mass

Positive effects of the adoption of a new breakup model come from the analysis of droplets diameter distribution in the spray, as already mentioned before. As can be observed in figure 5.12 the variation of injection conditions, either injection pressure or chamber counter pressure, reflects on the diameter distribution. The graphs are obtained considering a cross section of the spray at a certain axial distance from the injector tip (30 [mm] for P_r variations, 20 [mm] for P_k variations).



(a) Effects of Injection Pressure Variation (b) Effects of Chamber Pressure Variation

Figure 5.12: Effects of injection conditions on droplets diameter distribution

These curves are obtained considering the same values for SMD of initialization,

in order to observe the effects of the only injection and chamber pressures. As expected, these effects are visible on the graphs. The increase in injection pressure means a faster injected jet, which lead the droplets to reach in a shorter time the analysed cross section (red curve arise before blue curve in figure 5.12a) and to an improvement in the vaporization, which reflects in smaller droplets. On the other hand, an increase in chamber counter pressure slows down the spray propagation inside the chamber, thus a longer time is required for the first droplets to reach the studied cross section (figure 5.12b).

In order to understand up to which level the breakup and evaporation models should be relaxed to have acceptable results, some simulations have been performed in which the breakup models have been deactivated. This simulations also give further information about how much the fluid affects the spray propagation for increasing pressure and density. The considered case is the one with $P_r = 100$ [bar] and $P_k = 5$ [bar], and the results are shown in figure 5.13.

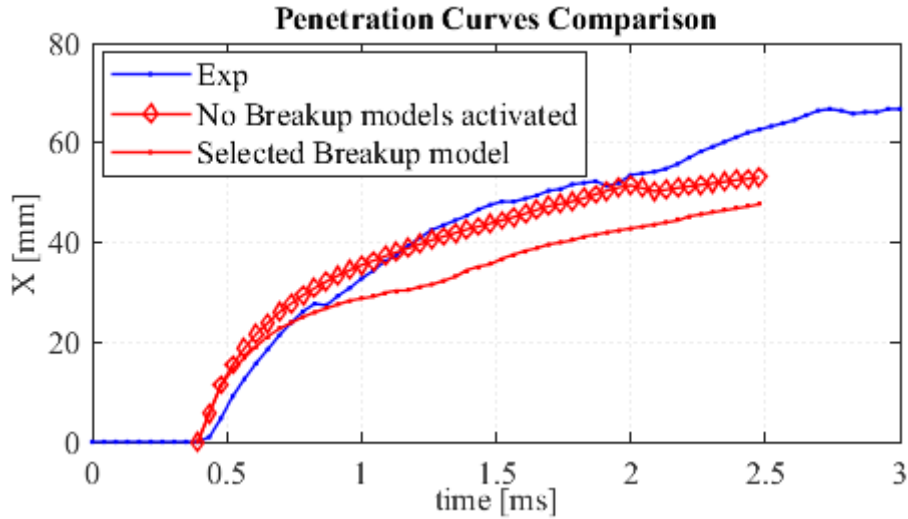


Figure 5.13: $P_r = 100$ [bar], $P_k = 5$ [bar] - Effects of breakup model deactivation

These results provide material for some interesting observations and considerations. First of all the simulation with breakup model deactivation provides very accurate approximation of experimental data in terms of geometry and kinematic of the spray, with an error lower than 10%. This means that the in-chamber conditions are so prone to facilitate the evaporation of the spray when the pressure increases that it would be necessary to not consider the secondary breakup of the droplets, but only the evaporation. Nevertheless this action should not be taken, since it has several undesired effects on other properties of the spray, apart from the kinematic properties, such as the SMD and the vaporized fuel mass distributions. Secondary

breakup is a phenomenon that must be taken into account to perform a simulation that provides a faithful reproduction of the physics of the spray, which is the key element in the application of injection simulation in the engine development, where the study of mixture formation is one of the key points.

In conclusion, this analysis of the models describing the spray breakup and atomization clarified that the software is extremely sensitive to in-chamber pressure variations, thus generating underestimated results in terms of spray penetration. A positive effect can be obtained by the adaptation of the droplet secondary breakup model to the pressure conditions, but it is questionable how much these model should be modified, and which level in the trade-off between spray geometry accuracy and spray physics coherence should be kept.

In the next section the possibility of further actions on the initialization diameter of the injected droplets is investigated to define which benefits can be obtained in terms of simulation quality.

5.4 Modification of SMD of Initialization

The last investigated solution for improving the quality of the simulations in terms of reproduction of the spray geometry and kinematic is the modification of the SMD of initialization. The values of SMD are modified up the point that the penetration curve from simulation fits the penetration curve obtained from experimental analysis. It is a goal of this analysis to find a correlation between the chamber counter pressure and the SMD of initialization that should be applied to obtain good approximation of the experimental results.

In the following the main results and considerations are reported, considering the cases of $P_r = 100$ [bar], $P_k = 5$ [bar] and $P_r = 100$ [bar], $P_k = 10$ [bar]. The starting point of this analysis are the results shown in figure 5.2.

The SMD of initialization of the injected droplet is characterized as before by a linear ramp during the first millisecond of the injection followed by constant initialization value for the remaining time.

Several simulations have been performed with different attempts for the initialization of the droplets SMD, and the final obtained results are shown in figure 5.14, while figure 5.15 graphically shows the found relation between chamber counter pressure and necessary values of SMD of initialization for obtaining an error between experimental and simulation curve lower than 10%.

The increase of SMD of initialization that allows to obtain acceptable results is not proportional to the increase in chamber counter pressure. In the two considered cases of $P_k = 5$ [bar] and $P_k = 10$ [bar] the values assumed by the SMD are reported in table 5.1.

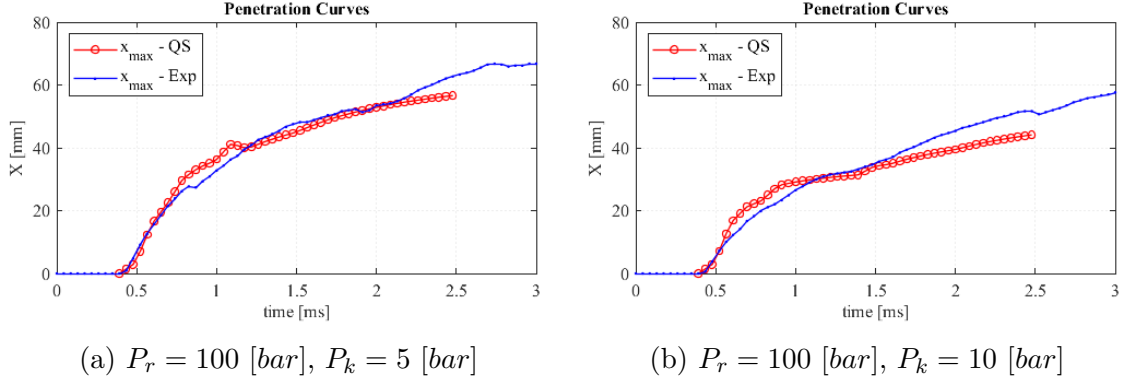


Figure 5.14: Penetration curves for simulations with adapted SMD of initialization

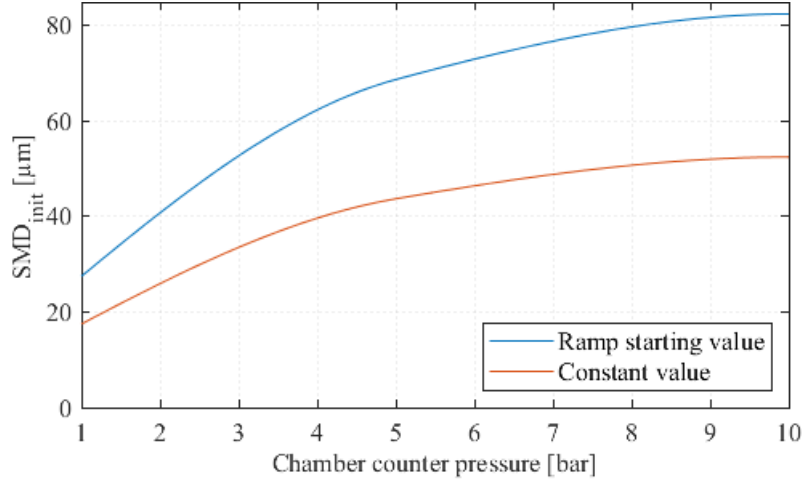


Figure 5.15: SMD of initialization as a function of chamber pressure

Even if this solution provides the best results from the point of view of geometry and kinematic of the spray, there are other factors that should be taken into account. The SMD distribution in the spray, as well as the quantity of vaporized mass during spray development and propagation are affected by this procedure.

Figure 5.16 shows the initialization diameter function and the droplets diameter distribution in the spray cross section at 30 [mm] from the injector tip.

	$P_k = 5$ [bar]	$P_k = 10$ [bar]
Initial value of the ramp [μm]	68.75	82.5
Constant value [μm]	43.75	52.5

 Table 5.1: SMD of initialization for best fitting - $P_r = 100$ [bar]

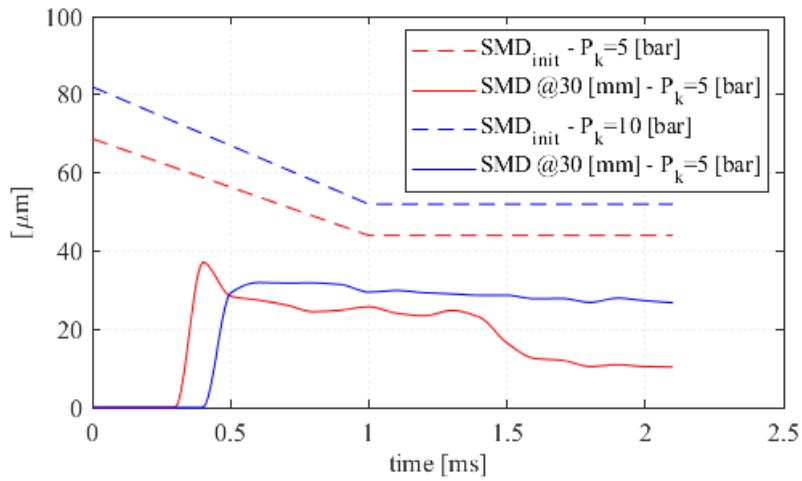


Figure 5.16: SMD of initialization and SMD distribution in a cross section of the spray at 30 [mm] from the injector tip

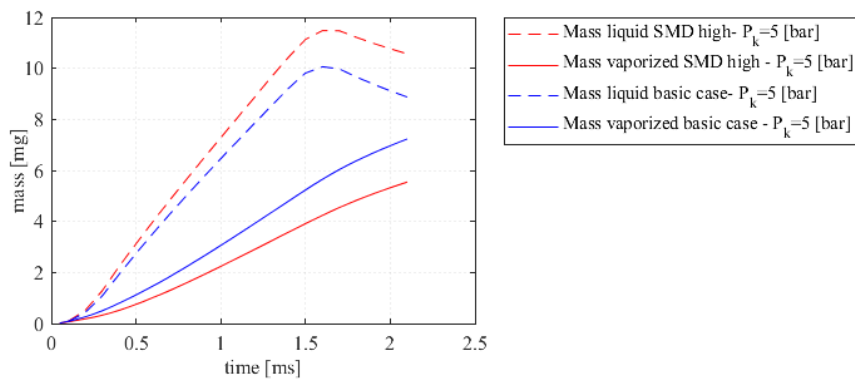


Figure 5.17: Example for $P_k = 5$ [bar] of Liquid and vaporized mass distribution - Comparison with the basic case

An increase in the size of the injected droplets allows the spray to penetrate deeper inside the chamber, but it is also a factor against the vaporization of the liquid fuel. In figure 5.17 it is demonstrated how the applied modifications cause a reduction of about 25% of the vaporized mass during injection.

This method for the initialization of the injected fuel is the most effective from the point of view of reproduction of spray development and propagation, but there are large variations in the behavior in terms of vaporization. Some considerations could be made about the level of accuracy that is required from the simulation, taking into account these variation in the physics of the spray that could have an influence on the further study of mixture formation in ICE simulations. Each simulation should be performed with the best possible setup based on what is its final goal.

A further way to validate this methodology for the definition of the injection model in a 3D-CFD environment can be its application in a complete internal combustion engine simulation, in which the complexity is enhanced by the presence of the piston movement and the turbulent motions, verifying the development of the spray and its propagation inside the chamber, the vaporization of the liquid fuel, the air/fuel mixture formation and distribution in the combustion chamber.

5.5 ICE Simulations

The new methodology developed for the definition of the injection model settings has been applied to a complete engine simulation, which adopts the studied type of multi-hole injector, in order to observe its influence and confirm its validity. The injected fuel initialization parameters and the droplets secondary breakup model have been modified according to the criteria exposed in the previous chapters. The main observed quantities are the fuel vaporized mass and the air/fuel ratio distribution, with particular focus on these quantities at ignition point. Considering injection conditions of $P_r = 150$ [bar] and $P_k = 1$ [bar], the injection parameters have been set as follows.

- Fuel exit speed: defined considering ideal speed from Bernoulli equation and experimental data about fuel exit speed

$$v_{exp} = 120 \text{ [m/s]}$$

$$v_{ideal} = 203.3 \text{ [m/s]}$$

The fuel exit speed is initialized considering a linear function between these two values along the whole injection period.

- SMD: the initial droplet size is evaluated considering the relation evaluated before and shown in figure 5.15. The Rosin-Rammler distribution parameters are not modified, and the number of droplets per parcel has been calculated accordingly.
- α angle: value defined according to injector manufacturer indications.
- Breakup model: KHRT model with values of the adjustable parameters $B_0 = 0.61$, $B_1 = 40$, $C_3 = 0.1$, $C_\tau = 9$.

In the studied case the injection duration is 50° , from $CA = 420^\circ$ to $CA = 470^\circ$, and the ignition point is at $CA = 708^\circ$.

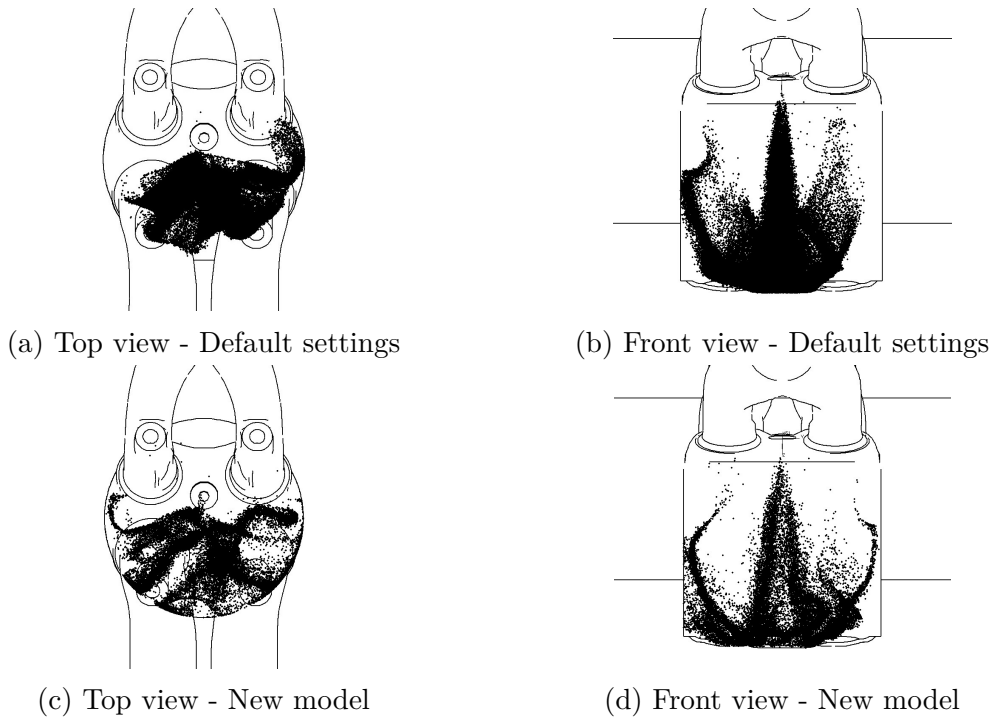


Figure 5.18: Spray propagation at End of Injection (EOI)

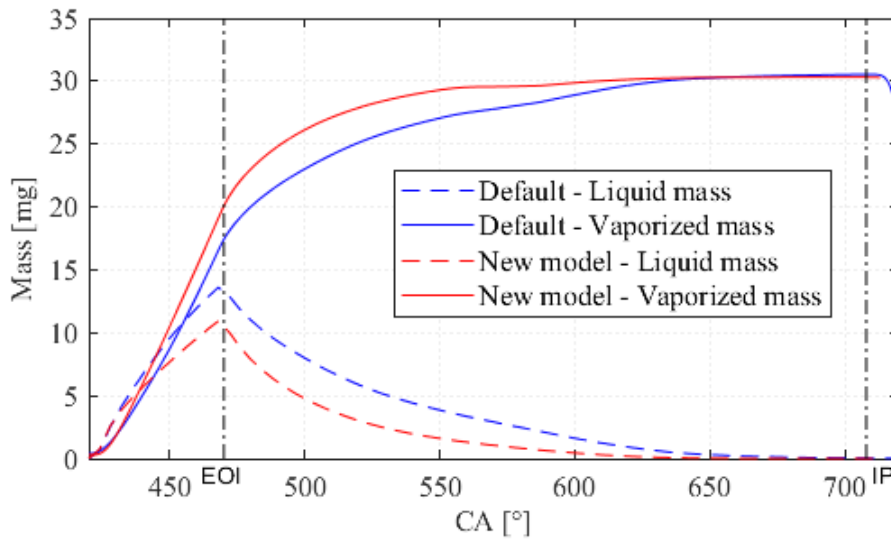


Figure 5.19: Liquid and Vaporized mass distributions

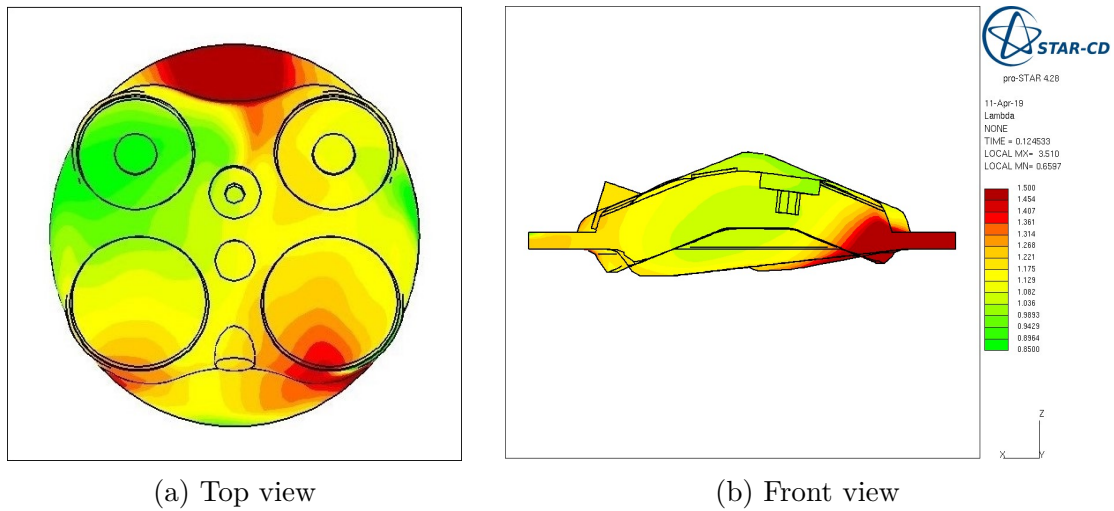


Figure 5.20: Lambda distribution at Ignition Point - Default settings

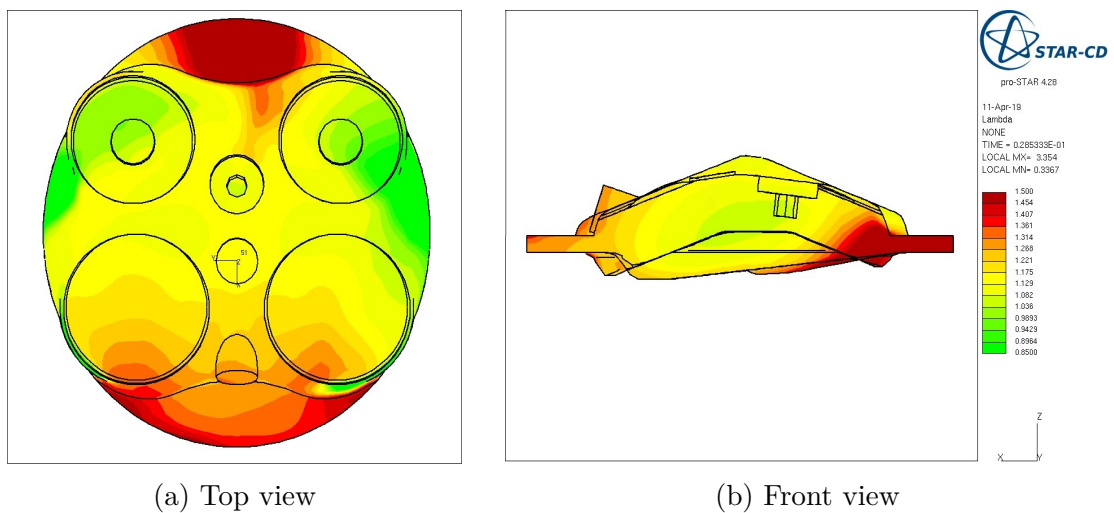


Figure 5.21: Lambda distribution at Ignition Point - New model

Figure 5.18 shows the spray propagation inside the combustion chamber at the end of injection, while The main results from the performed ICE simulations are reported in figures 5.20, 5.21, and 5.19, which report the distribution of air/fuel ratio λ and the vaporized mass distribution respectively.

The quantity of vaporized mass at ignition point is not affected by the applied modifications, being the injected fuel mass 30.59 [mg] and the vaporized mass at ignition point 30.5 [mg], which means approximately the 99% of the injected mass. The effects of the new model can be seen starting from the injection phase, where

the fuel seems to evaporate faster than the basic case.

The mixture formation is partially affected by the adoption of the new injection model, as can be seen in figures 5.20 and 5.21. The λ distribution at ignition point is generally characterized by a rich mixture in correspondence of the spark plug region, and a gradual transition to leaner mixture in the surrounding regions. What is different with the new model is not this characteristic mixture formation, but it is the size of the rich region around the spark plug, which is smaller.

Other properties that describes the in-chamber motions in preparation to the combustion seem not affected by the modification of the injection model.

The application of the new injection model appears not to have negative effects on the mixture formation process before combustion, although for final statements about the result of combustion and engine performance further more detailed analysis should be carried out. This confirms that the new developed model can provide good simulation of the injection event, both in studies of injection in constant volume chamber with quiescent environment, and in complete engine simulations with the presence of turbulent motions and piston movements.

Chapter 6

Conclusions and Outlook

The purpose of the present work was to develop a methodology for the definition of the injection model adopted by the 3D-CFD tool *QuickSim*, that would be able to improve the quality of the simulation. This has been possible by means of the combined use of the simulation tool and experimental tests data. The object of the study is an high-performance multi-hole injector for GDI applications working at injection pressure from 100 [bar] to 200 [bar].

The initial analysis of injection tests performed in a constant volume chamber at the test rig has been performed by means of an imaging tool appositally designed, and it has produced a consistent quantity of data related to the spray formation and development under different injection pressure conditions, that are able to describe the geometry and the kinematic behavior of the injected fuel spray in time. The results of this experimental analysis have been a key factor in the improvement of the injection model for simulation, in fact not only they have been used for a comparison between experimental and simulation results, but they have also been exploited to define rules for the initialization of the injection parameters in the CFD environment.

The 3D-CFD tool *QuickSim* requires the definition of a set of parameters describing the fuel droplets exiting the injector nozzle, since the peculiarity of this tool is that the internal nozzle flow and the primary droplets breakup phenomena are not object of the simulation, being the final goal of *QuickSim* to save computational time and provide a fast engine simulation tool applicable not only in research projects, but also in the engine development phase. The coupling of experimental tests results with the simulations plays a major role in the calibration of these parameters. In particular the fuel exit speed is the most suitable parameter to be adjusted according to the experimental results. As a matter of fact it has been initialized as a linear function over time between the ideal value calculated by means of the Bernoulli equation 3.3 and the value provided by the analysis of the experimental tests.

Among the other injection initialization parameters (spray angle, initialization domain, fuel properties, droplets SMD, etc.) the Sauter Mean Diameter of the injected droplets resulted as one of the most influential, but also one of the most challenging. The final choice was not to consider it constant during the whole injection, but to follow a ramp function in the first phase of injection and after that keeping it at a constant value. This solution was driven by the necessity of overcoming the lack in simulation of the fluidodynamics occurring until the primary droplets breakup. The results obtained in terms of spray reproduction and droplets diameter distribution during injection were very precise in the case considered as standard injection conditions ($P_r = 100$ [bar], $P_k = 1$ [bar]), with the difference between the experimental data and the simulation results for jet speed, spray angle, vertical penetration and axial penetration lower than 10%.

Some criticalities arose within a sensitivity analysis of the model to the application of an increase in chamber counter pressure. In this cases the shape of the spray was well reproduced by the simulations, but the results were characterized by a large underestimation of the spray penetration inside the chamber. This proved that the software models are highly dependent on the in-chamber air density, and the simulation tends to produce an environment more difficult for the spray to penetrate than the actual test chamber, hence the necessity of somehow adjusting the injection model to the injection conditions.

This high sensitivity of the simulation environment to in-chamber pressure conditions could be assessed as the main limit for the application of this model. Although several possible solutions have been investigated.

A detailed study of how the software manages the vaporization process of the injected fluid has been carried out, with particular focus on the secondary breakup phenomena. Among all the available droplets breakup model, the KHRT hybrid model has been selected as the one that best reproduce the experimental results, and it is also the most suitable for modification, as it presents four adjustable parameters which allow to set the level of droplets diameter reduction rate due to breakup and the breakup time, hence the possibility of define the aggressiveness of the breakup model according to the in-chamber pressure conditions.

Further improvements were obtained by means of the definition of a relation between chamber counter pressure and the initialization droplet size. This method allows to find the correct value of SMD of initialization for the droplets which is able to compensate the software's underestimations, and provides the fitting of simulation and experimental axial penetration curve, but also vertical penetration and spray angle. Even if this solution is the best in terms of reproduction of spray geometry and kinematic, it presents consequences in other properties of the spray such as droplets size distribution during injection and fuel vaporized mass distribution.

As it is possible to observe in figures 5.8 and 5.14, the developed injection model for *QuickSim* is able to correctly reproduce the injected fuel spray development and

propagation, without causing a significant increase in computational time with respect to the model previously adopted.

The validation of this model was completed by integrating it in a full internal combustion engine simulation over a complete cycle. An analysis of the air/fuel mixture formation has shown how the implementation of this new injection model does not lead to undesired side effects neither on the air/fuel ratio distribution, nor on the simulation of combustion.

The potential of this procedure has been proved with its application in a total different application. In particular it has been tested in a case which consider a different type of injector, injected fluid (water), and combustion chamber. The performed simulations in this water injection case have show the consistency of the whole procedure, starting from the calibration of simulation based on experimental data, and resulting in a realistic reproduction of the injection.

It has to be kept into consideration the fact that this injection model has been developed for the application in the 3D-CFD tool *QuickSim*, whose purpose is to provide a fast computational tool for virtual engine development process. Thus the adoption of specifically designed models for combustion, heat transfer, injection, etc., and a coarsening of the mesh structure allow sufficient savings in computational time, at the prize of an acceptable level of approximation, to make the simulation a powerful tool useful in every phase of the engine development process.

In this context it is clear that there is still margin for improvements in *QuickSim* simulations, especially for what concerns the definition of droplets breakup, and turbulence models, and also a more precise procedure for the initialization parameters definition based on the specific application case, in order to achieve a more realistic injection simulation under a variety of injection conditions.

Bibliography

- [1] A.H. Lefebvre, V.G. McDonell *Atomization and sprays*, CRC Press, 2017.
- [2] N. Mitroglou, *Multihole injectors for Direct-Injection Gasoline engines*, PhD thesis, City University of London, 2006.
- [3] N. Mitroglou, J.M. Nouri, M. Gavaises, C. Arcoumanis, *Spray characteristics of a multi-hole injector for Direct-Injection Gasoline engine*, Internal journal of engine research, 2006.
- [4] N. Ding, *Spray characteristics of new generation multi-hole injector for spark-ignition gasoline engines with direct fuel injection*, WASE International conference on information engineering, 2010.
- [5] M. Wentsch, *Analysis of injection processes in an innovative 3D-CFD tool for the simulation of internal combustion engines*, PhD thesis, Stuttgart University, 2017.
- [6] M. Chiodi, *An innovative 3D-CFD-Approach towards virtual development of internal combustion engines*, Vieweg+Teubner Research, 2011.
- [7] J.Y. Tan, F. Bonatesta, H. Kiat Ng, S. Gan, *Developments in computational fluid dynamics modelling of gasoline direct injection combustion and soot emission with chemical kinetic modelling*, Applied thermal engineering, 2016.
- [8] CD-adapco, *Star-CD - Methodology, Commands, User guide v4.18*, 2012.
- [9] Robert Bosch GmbH, [Online] <https://www.bosch-mobility-solutions.com>, 2018.
- [10] F. Millo, M. Badami, A. Bianco, E. Delogu, *CFD Diagnostic methodology for the assessment of mixture formation quality in GDI engines*, SAE International Journal Engines Vol. 4, 2011.
- [11] M. Badami, V. Bevilacqua, F. Millo, M. Chiodi, M. Bargende, *GDI swirl injector spray simulation: a combined phenomenological-CFD approach*, SAE technical paper series, 2004.
- [12] S. Sazhin, *Droplets and sprays*, Springer-Verlag London, 2014.
- [13] R.D. Reitz, *Modeling atomization processes in high-pressure vaporizing sprays*, Elsevier applied science publishers Ltd, 1987.
- [14] J.C. Beale, R.D. Reitz, *Modeling spray atomization with Kelvin-Helmholtz/Rayleigh-Taylor hybrid model*, 1999.
- [15] K. Saha, S. Som, M. Battistoni, Y. Li, S. Quan, P.K. Senecal, *Modeling of*

- internal and near-nozzle flow for a gasoline direct injection fuel injector*, ASME Journal of energy resources technology, 2016.
- [16] A. Sabau, M. Barhalescu, E. Oanta, *Modeling of high-pressure fuel injection systems*, Annals and proceedings of DAAAM, 2012.
- [17] P. Cwikowski, P. Jaworski, A. Teodorczyk, *Comparison of break-up models in simulation of spray development in direct injection SI engine*, Journal of KONES Powertrain and transport, 2010.
- [18] S. Sazhin, W.A. Abdelghaffar, E.M. Sazhina, M.R. Heikal, *Models for droplet transient heating: effects on droplet evaporation, ignition, and break-up*, International journal of thermal science, 2005.
- [19] SAS IP, [online] <https://www.sharcnet.ca>, 2018.
- [20] S. Lee, S. Jeong, O. Lim, *An investigation on the spray characteristics of DME with variation of ambient pressure using the common rail fuel injection system*, Journal of mechanical science and technology, 2012.
- [21] M. Pilch, C.A. Erdman, *Use of breakup time data and velocity history data to predict the maximum size of stable fragments for acceleration-induced breakup of a liquid drop*, International journal of multiphase flow, 1987.
- [22] A. Twellmeyer, F. Köpple, B. Weigand, *A novel CFD approach for modelling the high-pressure direct injection and mixture formation in a sprak-ignited CNG engine*, International journal of computational methods and experimental measurements, 2016.